Received: 14 February 2021 | Revised: 20 October 2021 | Accepted: 25 October 2021

DOI: 10.1002/dep2.172

The Depositional Record Open Access
A journal of the International Association of Sedimentologists
IAS WILEY

ORIGINAL ARTICLE

The Steptoean Positive Carbon Isotope Excursion (SPICE), inorganic aragonite precipitation and sea water chemistry: Insights from the Middle–Late Cambrian Port au Port Group, Newfoundland

Joyce E. Neilson[1] | **Rosalia Barili**[2] | **Alexander Brasier**[1] | **Luiz F. De Ros**[3] | **Sarah Ledingham**[1]

[1]University of Aberdeen, Aberdeen, UK
[2]PUCRS, Porto Alegre, Brazil
[3]UFRGS, Porto Alegre, Brazil

Correspondence
Joyce E. Neilson, School of Geosciences, University of Aberdeen, Meston Building, Aberdeen AB24 3UE, UK.
Email: j.neilson@abdn.ac.uk

Funding information
Aberdeen Formation Evaluation Society; Shell Brazil; University of Aberdeen

Abstract

The Late Cambrian Steptoean Positive Carbon Isotope Excursion marks a time of significant change in ocean chemistry and trilobite faunas. On the lead up to the carbon isotope excursion and at the excursion itself, there is global evidence from Laurentia and Gondwana of cementation by primary aragonite in shallow subtidal environments accompanied by deposition of aragonitic ooids. However, this occurred at a time widely considered to have been characterised by 'calcite seas' when the primary inorganic phases (marine cements and ooids) are normally presumed calcitic. This study has investigated the chemostratigraphy of the Middle–Late Cambrian Port au Port Group, Newfoundland, including the early marine cements. Here, the marine cements contain increasing concentrations of strontium towards the peak carbon isotope excursion (up to 5500 ppm at the peak excursion) before dropping off post-peak excursion, consistent with the original cements having been aragonitic. This trend is accompanied by relict oomouldic porosity, again suggesting an aragonitic precursor. Primary inorganic mineralogy is largely controlled by the Mg/Ca ratio of sea water but estimates of the Mg/Ca ratio of Late Cambrian oceans are variable (0.8–2). At this level, other factors such as water temperature and pCO_2 have been shown to affect mineralogy with warm waters and high levels of CO_2 favouring aragonite. It is possible that the warm waters and anoxia that caused the carbon isotope excursion created conditions favourable for the precipitation of aragonite at the same time as major trilobite faunal turnover.

KEYWORDS

aragonite, Cambrian, chemostratigraphy, SPICE, strontium

1 | INTRODUCTION

The Cambrian was a time of significant evolution of life in the oceans with not only two major evolutionary explosions (Phase 1 and 2) but also extinctions during the Sinsk event and, much more significant, at the Steptoean Positive Carbon Isotope Excursion (SPICE) in the Late Cambrian (Furongian) (Zhuravlev & Wood, 2018). The SPICE (Saltzman et al., 1998) is a global carbon isotope excursion with $\delta^{13}C$ values typically *ca* 4–5‰ although values can be lower (Pulsipher et al., 2021).

In a study of Furongian marine cements from the Al Bashair Formation, Oman (Gondwana), Neilson et al. (2016) concluded that conditions suitable for the precipitation of aragonite and high-Mg calcite (HMC) may have existed around the SPICE, a time generally believed to be of stable 'calcite' seas (Stanley et al., 2010). Understanding the chemistry and conditions of sea water at the time is therefore critical.

The mineralogy of inorganic carbonate precipitates is largely controlled by the Mg/Ca ratio of sea water (Hardie, 1996; Lowenstein et al., 2001) with Mg/Ca ratios >2 favouring the precipitation of aragonite and ratios <2 favouring calcite. Temperature and pCO_2 have also been shown to have an effect, especially within a Mg/Ca range of 1–2 (Balthasar & Cusack, 2015). The estimates of Mg/Ca ratios during the Late Cambrian range from 0.8 to 2 (Arvidson et al., 2006; Horita et al., 2002; Stanley et al., 2010).

The Middle–Late Cambrian Port au Port Group in Newfoundland (Laurentia), also records the time leading up to and around the SPICE and contains significant information about sea water conditions and chemistry. It presents an ideal opportunity to test the hypothesis that inorganic aragonite and/or HMC could have precipitated on a global scale during the Middle–Late Cretaceous. Evidence of relict Late Cambrian aragonite ooids has also been found in the Johns Wash Limestone (Conley, 1977) and the Open Door Formation, Wyoming (Martin et al., 1980).

According to Chow (1985), the first studies of the Cambrian Series 3—Furongian Port au Port Group (PAP), Port au Port Peninsula, Western Newfoundland (Figures 1 and 2), date back to Logan (1863) and Schuchert and Dunbar (1934). Several studies followed, gradually improving sedimentological and biostratigraphic knowledge. Chow (1985) produced one of the most complete studies to date, integrating the stratigraphy, sedimentology and diagenesis of the PAP (Figure 1). It was also the first to conduct stable isotope analysis. This was followed by Chow and James (1987a, 1987b), and later by Cowan and James (1993) who revisited the stratigraphic sections and published a refined sedimentological interpretation.

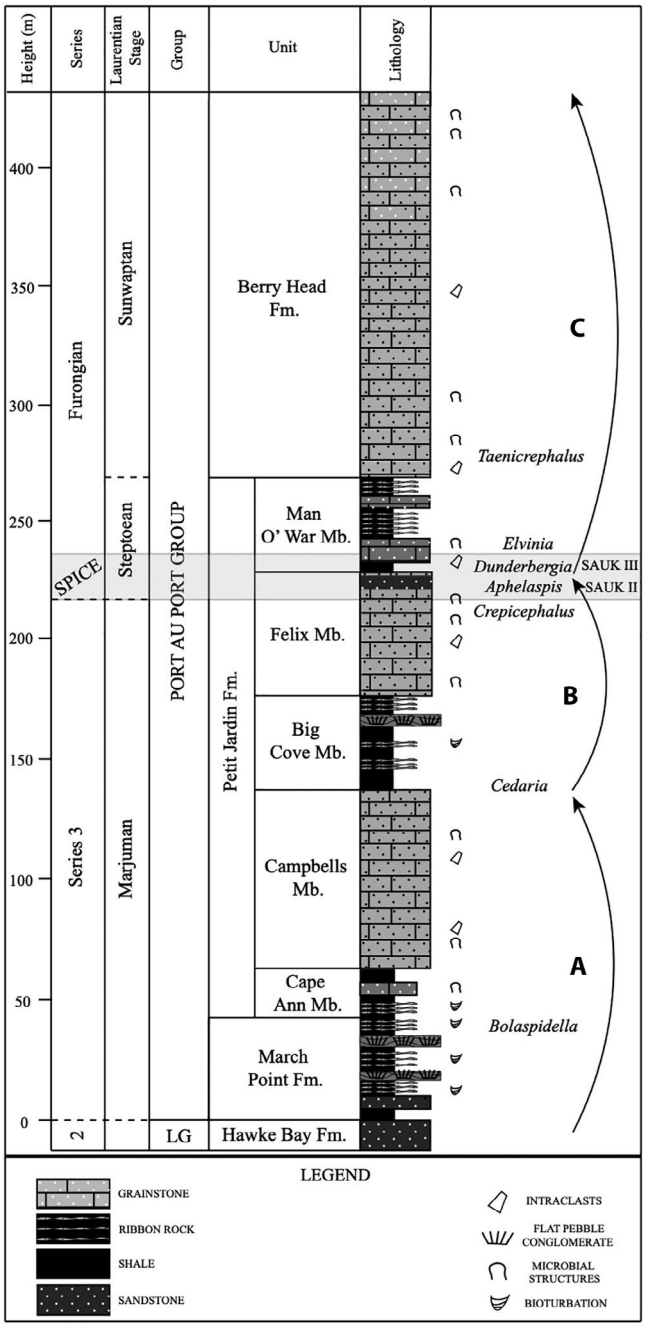

FIGURE 1 Schematic stratigraphic log of the Port au Port Group based on thicknesses logged in this study in the March Point and FCSs (after Chow, 1985; Cowan & James, 1993). Each of the Grand Cycles (A, B and C) consists of a lower interbedded clean and shaley ribbon rock half-cycle and an upper oolitic half-cycle. The estimated Sauk II-III boundary coincides with the SPICE (Barili et al., 2018; Saltzman et al., 2004). LG, Labrador Group

A subsequent study at Felix Cove (Figure 2) by Saltzman et al. (2004), showed that the SPICE occurs towards the top of the Petit Jardin Formation (PJF) and is coeval with a major change in trilobite fauna (Figure 1). Subsequently, the SPICE was also identified in the March Point Section (MPS; Figure 3) by Hurtgen et al. (2009) in a

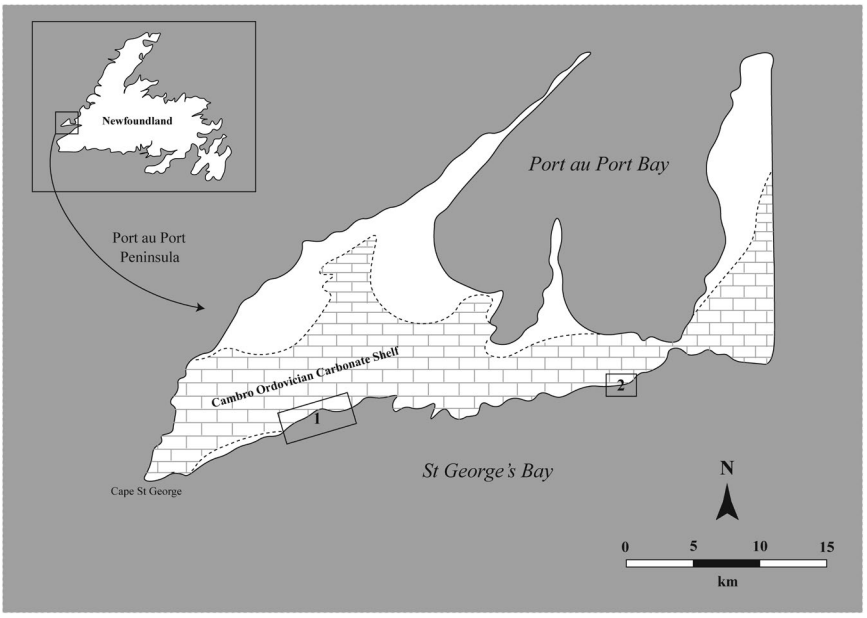

FIGURE 2 Study area in the Port au Port Peninsula, Western Newfoundland. Location of the logged sections are highlighted: March Point (1) and Felix Cove (2) sections

paper focussed on carbon and sulphur isotopes. The presence of the SPICE was later confirmed at both localities by Barili et al. (2018). Limited lithofacies information and no petrographic data were presented by Saltzman et al. (2004) or Hurtgen et al. (2009) but was added by Barili et al. (2018).

This paper presents a detailed petrographic and geochemical study through the most complete section of the PJF (MPS) together with the Felix Cove section (FCS; Figure 2). The petrographic and isotopic study by Barili et al. (2018) allowed the correlation of the SPICE and its associated sedimentological interval through the Port au Port Peninsula. The present study adds X-ray fluorescence elemental concentration data and extensive microprobe analyses of the early marine cements found in the PJF. This allowed the construction of a detailed chemostratigraphy for the Middle Cambrian Series 3 and Late Cambrian Furongian on the Port au Port Peninsula and, through investigation of the early marine cements, provides important information regarding oceanic chemistry at the time.

2 | GEOLOGICAL SETTING

The study area is located on the southern coast of the Port au Port Peninsula, western Newfoundland (Figure 2). The PAP is interpreted as being of shallow-marine origin, deposited on the outer area of a stable carbonate platform adjacent to the Iapetus Ocean (Cowan & James, 1993; Palmer & James, 1979; Williams, 1979). These predominantly carbonate deposits, with episodic siliciclastic incursions, record the gradual transition from siliciclastic deposition in Cambrian Series 2 (Hawke Bay Fm., Labrador Group) to predominantly carbonate sedimentation in the early Ordovician (Chow, 1985; Chow & James, 1987b; Cowan & James, 1993). The Group is composed of three formations, namely the March Point Formation (MPF), PJF (Cape Ann, Campbells, Big Cove, Felix and Man O' War members) and Berry Head Formation (Figure 1).

Chow and James (1987a) defined three Grand Cycles through the PAP (Figure 1A–C), which they interpreted as transgressive–regressive sedimentary packages with a mixture of shallow subtidal–intertidal sedimentation. In a re-interpretation of the sequence, however, Cowan and James (1993) suggested that most sedimentation occurred in the subtidal environment in stacked ribbon rock and oolite shelf cycles separated by very thin peritidal horizons. The thin, wavy and lenticular bedded ribbon rock was defined by Cowan and James (1993) as consisting of nodular and parted limestone, with shale interbeds and abundant intraformational flat pebble conglomerates (FPCs).

The SPICE was identified by Saltzman et al. (2004) at Felix Cove and in the MPS by Hurtgen et al. (2009). Barili et al. (2018) identified the precise locations of these excursions as 48°31′49.2″N/58°47′12″W in Felix Cove and at 48°30′42.1″N/59°05′31.1″W in the MPS. Stratigraphy suggests that a potential third locality may exist on the coastline between the FCS and MPS at 48°30′25.6″N/59°06′29.9″W, although no geochemical data are available (Barili et al., 2018).

3 | METHODS

3.1 | Sedimentogical logs and petrography

Two outcrop sections on the Port au Port Peninsula were logged and sampled at March Point and Felix Cove (Figure

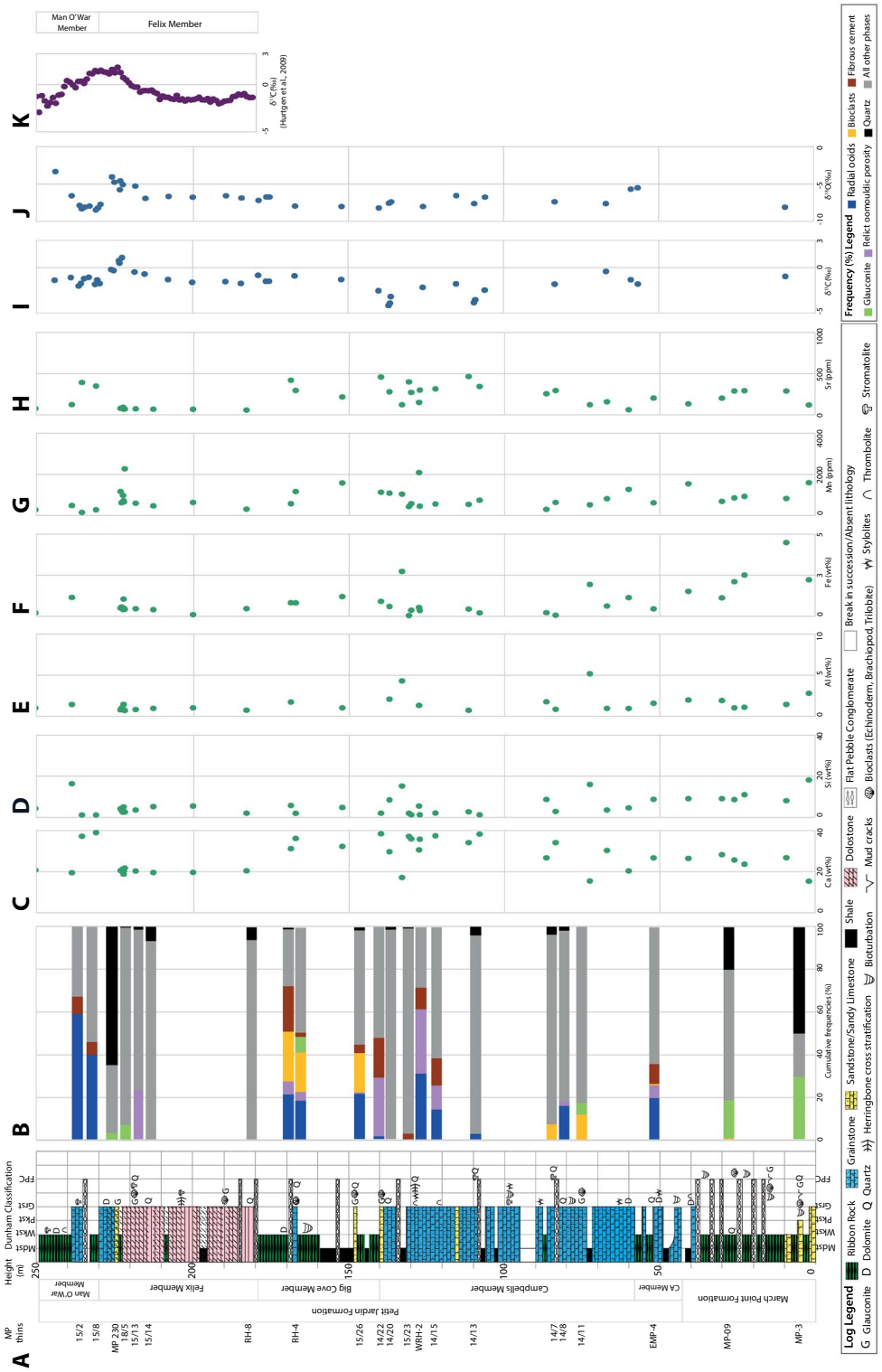

FIGURE 3 MPS. (A) Summary lithological log. (B) Point count frequency (%) of phases. (C–H) pXRF elemental analysis. (I–J) Isotopic analysis. (K) Data of Hurtgen et al. (2009)

2). To provide a stratigraphic framework for geochemical analysis, sedimentological logging was conducted on a centimetre scale (1:50). Systematic sampling at metre intervals was performed from the base of accessible units in the MPF and PJF (Figure 1) to the top of the accessible sections at March Point and Felix Cove (Cunha, 2019). The stratigraphic section logged at the MPS (Figure 3) was 270 m thick while the section at Felix Cove (FCS, Figure 4) was 40 m thick.

Representative layers were selected for thin-section preparation (MPS: 70; FCS: 31). Polished thin-sections, impregnated with blue resin for porosity identification, were prepared at the Universidade Federal do Paraná and the University of Aberdeen (UoA). Petrographic analysis was performed at the UoA and Universidade Federal do Rio Grande do Sul (UFRGS). For identification of the carbonate minerals, thin-sections were stained with a solution of alizarin red and potassium ferrocyanide (Dickson, 1965) at UFRGS. All thin-sections made at the UoA were polished and unstained. Point count data were collected at UoA using six digital photomicrographs from each thin-section taken at regular positions. A grid overlay of 25 intersections at 500 μm enabled regular and accurate point counting with $n = 150$.

3.2 | pXRF analysis

Portable XRF (pXRF) techniques were used to determine the bulk composition of the various units in the PJF (e.g. limestone, extent of dolomitisation and siliciclastic layers). Bulk powder samples were analysed for their elemental composition using an Olympus InnovX portable XRF instrument and InnovX software at the UoA. A total of 40 samples from the MPS and 20 from FCS section were analysed. Each sample was run twice through the geochemistry mode to calculate an average. The instrument was calibrated at the beginning of each run using a steel calibration check disc, with standards and a SiO_2 blank (Olympus). The pXRF data were further calibrated using an UoA sample database (40 Precambrian shales) analysed by both pXRF and ICP-MS. The relative standard deviation for the elemental analysis was: Mg (18.44%), Al (4.46%), Si (3.89%), Ca (2.05%) and Sr (0.77%). The technique is more accurate for Ca compared to Mg which is at the low-energy region of the spectrum (Hall et al., 2014). Calcium is therefore a better indicator of the degree of dolomitisation than Mg for the carbonate layers of the PJF.

3.3 | Electron microprobe analysis

Electron microprobe analysis was conducted at the Edinburgh Probe Microanalysis facility (UK). Sixteen polished thin-sections were analysed for Sr (detection

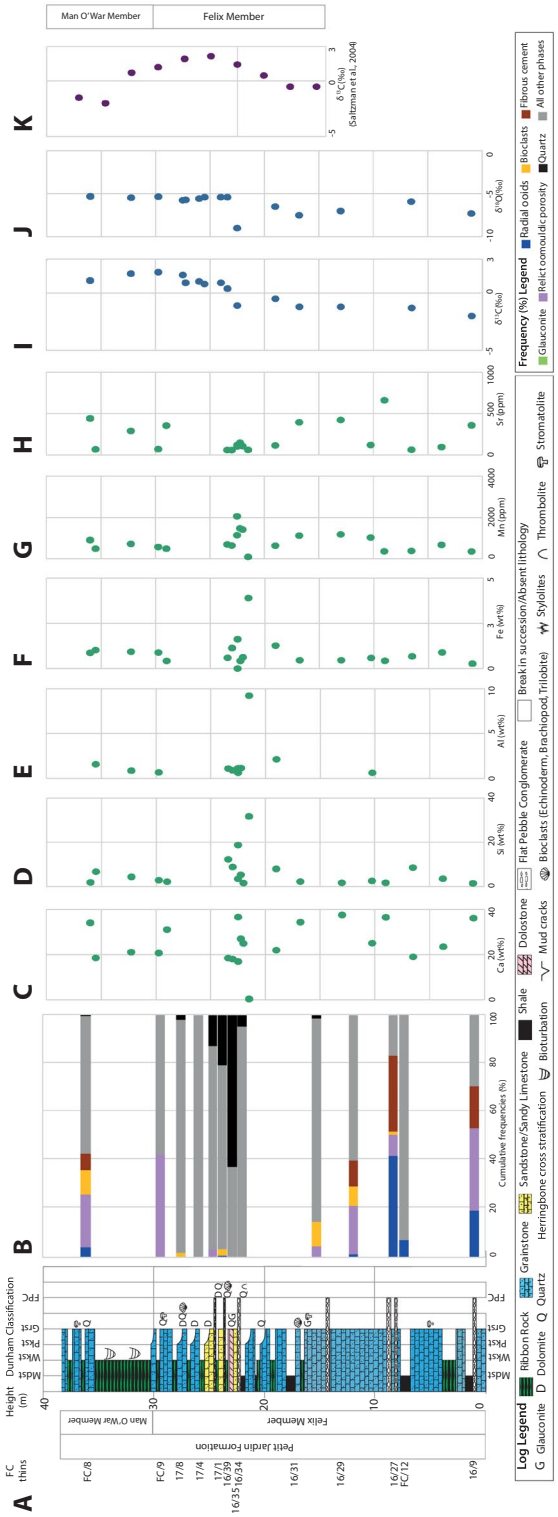

FIGURE 4 FCS. (A) Summary lithological log. (B) Point count frequency (%) of phases. (C–H) pXRF elemental analysis. (I–J) Isotopic analysis. (K) Trend of Saltzman et al. (2004)

limit 70 ppm, standard deviation <0.01%), Mg (detection limit 60 ppm, standard deviation <0.01%), Ca (detection limit 1600 ppm, standard deviation 0.6%), Mn (detection limit 230 ppm, standard deviation <0.02%) and Fe (detection limit 250 ppm, standard deviation <0.02%). A 5 μm diameter 15 KV beam, was employed. Calcium was measured with a 2 nA current and all other elements with a 60 nA current.

4 | RESULTS

4.1 | Sedimentology

The MPS and FCS exposing the MPF and PJF were originally logged by Chow (1985) where bases and tops of units were identified and characterised. These boundaries were used to help identify the different formations and members during this study.

4.1.1 | March point section

March Point Formation (0–43 m)

The lower part of the MPF comprises sandy limestone with glauconite and bioclast (trilobite, brachiopod and echinoderm) fragments associated with ribbon rock (Figures 3 and 5A—mixed shale and calcisiltite *sensu* Cowan & James, 1993). Above this, bioturbated ribbon rock with whole brachiopod shells and syneresis cracks (Figure 5C) is interbedded with FPC, containing rip-up clasts of mudstone fragments like those found elsewhere in the sequence (Figure 5D). At the top, the formation includes partially dolomitised oolitic grainstones and thrombolites interbedded with thicker (up to 2 m) layers of shale (Figure 3). Thin-sections show that the sandy grainstones are glauconitic-rich with minor bioclastic fragments (echinoderm, brachiopod and trilobite, Figure 5B). No early isopachous, fibrous cements or relict oomouldic porosity are observed.

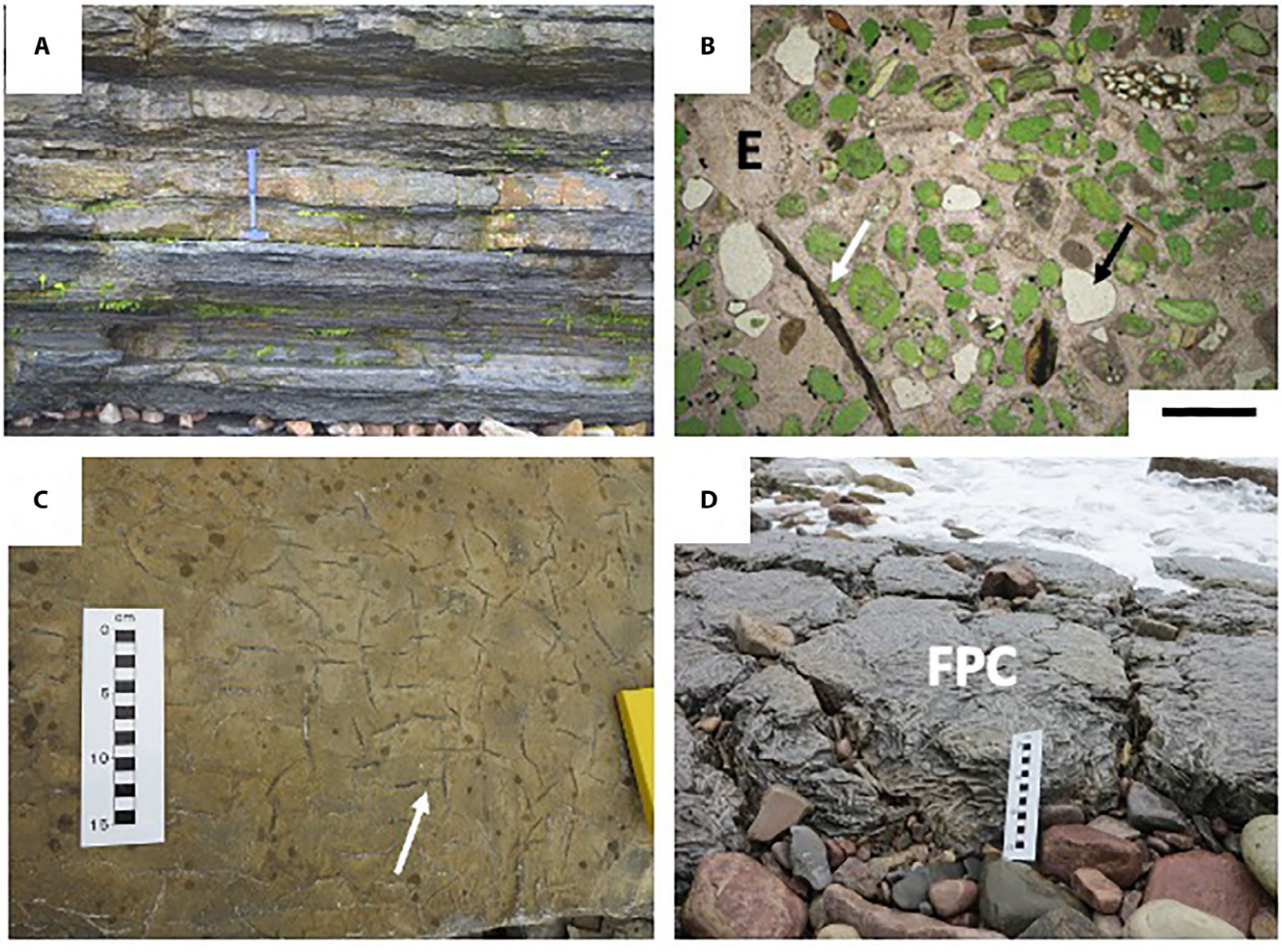

FIGURE 5 Outcrop and thin-section images. (A) March Point Fm. (MPS, *ca* 10 m). Glauconitic sandy limestone ribbon rock. Hammer 0.4 m. (B) March Point Fm. (MPS, 9.25 m). Poorly sorted quartz (black arrow), glauconite (green), bioclastic limestone with echinoderm (E) and brachiopod (white arrow) fragments. Stained thin-section, scale bar 500 μm. (C) March Point Fm. (MPS, *ca* 15 m). Subaqueous diastasis cracks (white arrow). (D) Big Cove Mbr. (MPS, *ca* 155 m). Randomly orientated lithoclasts in flat pebble conglomerate (FPC)

Chow (1985) placed the lower boundary of the MPF as the unconformity with a massive sandstone of the Hawke Bay Formation (part of the Labrador Group, Cambrian Series 2, Figure 1). The upper boundary is defined by a distinctive round pebble conglomerate bed (Figure 3).

Petit Jardin Formation–Cape Ann Member (43–58 m)

The Cape Ann Member comprises shale (variable bioturbation), ribbon rock and oolitic grainstones (Figure 6A). Although bioturbation is common in the fine sediments, bioclasts (e.g. echinoderm fragments) are rare or absent, occurring only as the nuclei of ooids. Thin-section analysis of grainstones shows early isopachous, fibrous cements throughout. A small amount of relict oomouldic porosity is observed but radial ooids dominate (Figures 3 and 6B).

Chow (1985) placed the lower boundary as the grainstone that immediately overlies the rounded pebble conglomerate bed that marks the top of the MPF. The upper boundary was recorded as the highest occurrence of interbedded silty limestone, dolostones and shale that underlies the thick-bedded grainstones/dolostones of the Campbells Member.

Petit Jardin Formation—Campbells Member (58–140 m)

The Campbells Member is a thick sequence comprising several sets of oolitic grainstones interbedded with minor ribbon rock and bioturbated shale (Figure 6C). Occasional glauconite and increasing bioclast fragments (echinoderm, brachiopod and trilobite) are observed (Figure 3). In the upper part of the formation, microbial structures (thrombolites and stromatolites) occur, often overlying FPCs. In the upper 40 m, oolitic grainstones can display herringbone stratification together with occasional sandy limestone layers. In thin-section, oolitic grainstones can display early isopachous fibrous cement

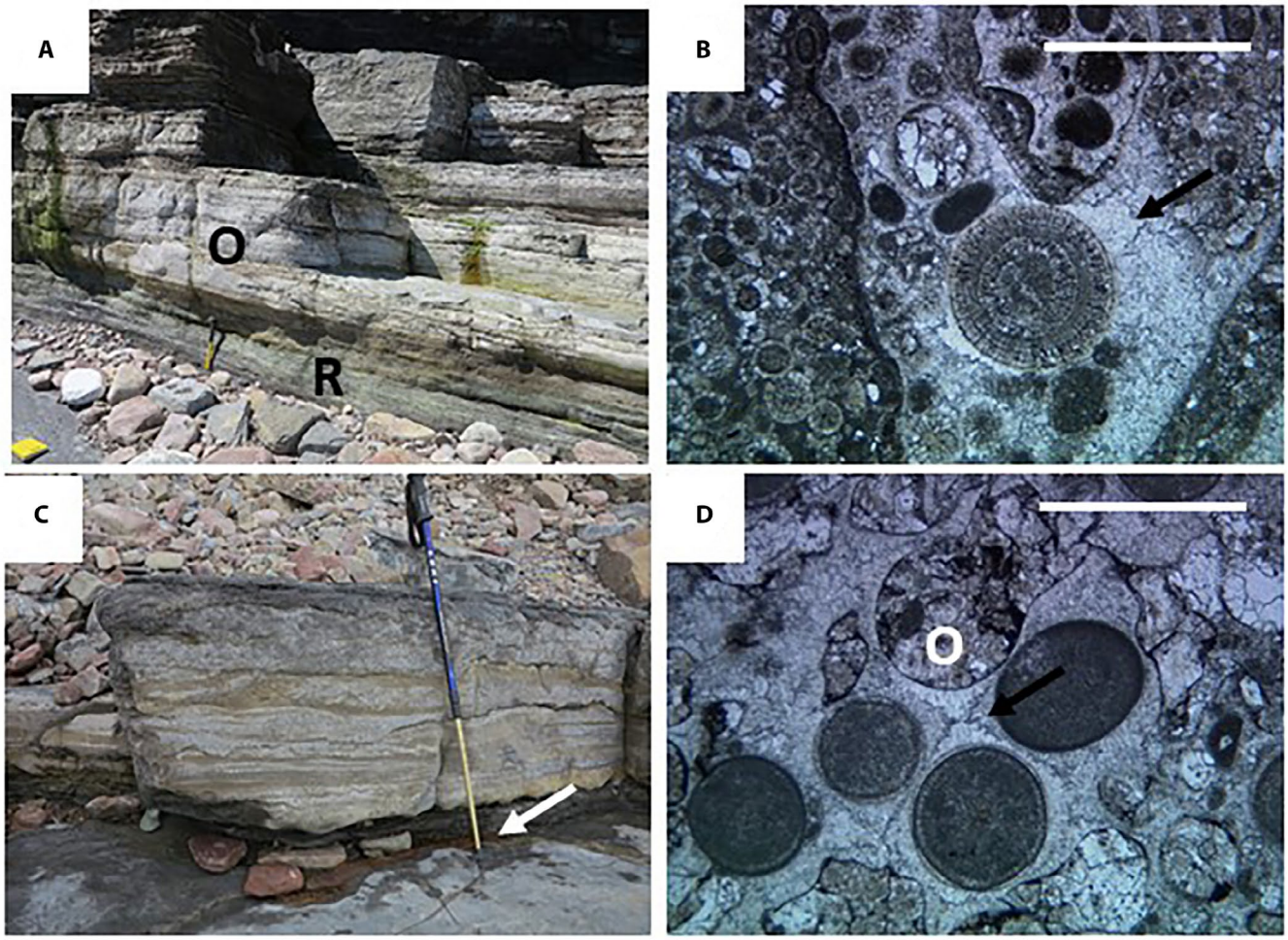

FIGURE 6 Outcrop and thin-section images (scale bars 1000 μm). (A) Cape Ann Mbr. (MPS, *ca* 50 m). Ribbon rock (R) overlain by oolitic and intraclast grainstones (O). Hammer 0.48 m. (B) Cape Ann Mbr. (MPS, 54 m). Intraclastic-oolitic-peloidal grainstone with minor isopachous, fibrous fringe cement surrounding ooids (arrow). (C) Campbells Mbr. (MPS, *ca* 100 m). Massive bedded oolitic grainstone with thin shale interbeds (arrow). Pole 1 m. (D) Campbells Mbr. (MPS, 108 m). Oolitic-peloidal grainstone with well-developed fibrous fringe cements (arrow). Relict oomouldic porosity (O) is observed, filled by dolomite

fringes throughout the Campbells Member with grainstones in the upper Campbells Member (above 107 m), displaying increased amounts of relict oomouldic porosity (Figures 3 and 6D).

Chow (1985) placed the lower boundary of this member at the base of the thick-bedded grainstones that overlie the ribbon rock of the Cape Ann Member with the upper boundary being the highest occurrence of thick-bedded oolitic grainstones. Above the oolitic grainstones, a fine, intraclast and sandy grainstone layer occurs immediately below a 1.5 m thick brachiopod-rich shale. The current study has placed the boundary between the Campbells and the Big Cove members at this level (140 m).

Petit Jardin Formation—Big Cove Member (140–179 m)

The Big Cove Member is dominantly composed of ribbon rock, interbedded with shale. The base of the Big Cove Member is marked by a prominent brachiopod-rich shale overlain by ribbon rock. Periodic layers of FPC (Figure 5D) and bioclastic grainstones (echinoderm, brachiopod and trilobite fragments, Figure 7A) with glauconite and occasional incursions of sandy limestone are observed throughout the member. In thin-section, bioclastic grainstones can display early isopachous fibrous cement fringes (Figure 7B). Radial ooids dominate with some relict oomouldic porosity (Figure 3).

Chow (1985) placed the lower boundary above the thick oolitic grainstones of the Campbells Member. As noted above, a prominent brachiopod-rich shale occurs at this level marking the base of the Campbells Member. Chow (1985) placed the upper boundary at the highest occurrence of thin-bedded parted limestones (ribbon rock *sensu* Cowan & James, 1993) below the thick-bedded dolostones of the overlying Felix Member. This can be recognised in the field by a FPC which underlies dolomitised grainstones at 179 m.

Petit Jardin Formation—Felix Member (179–230 m)

The Felix Member comprises pink–grey dolostones and partially dolomitised oolitic grainstones, interbedded with ribbon rock and shale (Figure 7C). Herringbone and low-angle stratification occurs above 201 m, with several layers of stromatolites and the occasional presence of bioclasts (trilobite and echinoderm fragments) (Figure 3). A prominent digitate stromatolite layer occurs at 222.25 m (Figure 8A), which trapped coated echinoderm grains, fine sub-rounded quartz grains and ooids (relic oomouldic porosity filled with dolomite, Figure 8B). This is overlain by a fine, quartz-rich, glauconitic dolomite (Figure 8C) with occasional fine sub-rounded quartz grains (Figure 8D). Elsewhere in the Felix Member, in thin-section much of the original texture has been masked by dolomitisation (Figure 7D) but early isopachous fibrous cement fringes in grainstones can be observed below 209 m and relict oomouldic porosity filled with dolomite occurs from 215 to 225.5 m.

Chow (1985) placed the lower boundary of this unit at the junction between the thin ribbon rock of the underlying Big Cove Member and thicker bedded dolostones of the Felix Member. As noted above, in this study a FPC was observed underlying the thick-bedded dolostones. Chow (1985) observed that the upper boundary is marked by thick-bedded grainstones/dolostones overlain by parted limestones (ribbon rock *sensu* Cowan & James, 1993).

Petit Jardin Formation—Man O'War Member (230 m upwards)

The Man O'War Member comprises grainstones, packstones and microbial structures (thrombolites and stromatolites) interbedded with ribbon rock and shale (Figures 3 and 7E). In thin-section, non-dolomitised oolitic grainstones at the base of the member display early isopachous cement fringes but no relict oomouldic porosity, with oolitic grains retaining original radial and tangential fabrics (Figure 7F).

Chow (1985) placed the lower boundary at the highest occurrence of the thick-bedded dolostones of the Felix Member. The upper boundary was not logged in the MPS as the section becomes more difficult to follow along the coast.

4.1.2 | Felix Cove Section

A smaller section of the PJF is exposed at Felix Cove with only parts of the Felix and Man O'War members outcropping (Figures 4 and 9).

Petit Jardin Formation—Felix Member (up to 30 m)

The base of the Felix Member is not exposed in the FCS. The section comprises oolitic grainstones interbedded with minor ribbon rock, shale and FPCs. Towards the top of the member (19–22.5 m), several fining-upward grainstone—shale cycles, ranging between 0.5 and 1 m, are present. These are capped by a low relief, oblate thrombolite layer at 22 m (Figure 9D) which has been dolomitised and contains fine, sub-rounded quartz grains (Figure 9E). This is overlain at 22.5 m by a coarse-grained sandstone with minor glauconite displaying low-angle, planar cross-bedding and coincides with the onset of the SPICE (Figures 4 and 9A,C). Above this, partially dolomitised fining-up grainstone–shale cycles continue (23.5–28 m). Quartz-rich grainstones occur up to 30 m (Figure 9B), together with pedestal thrombolites at the top of the member. Thin-section analysis of the sandy limestones show

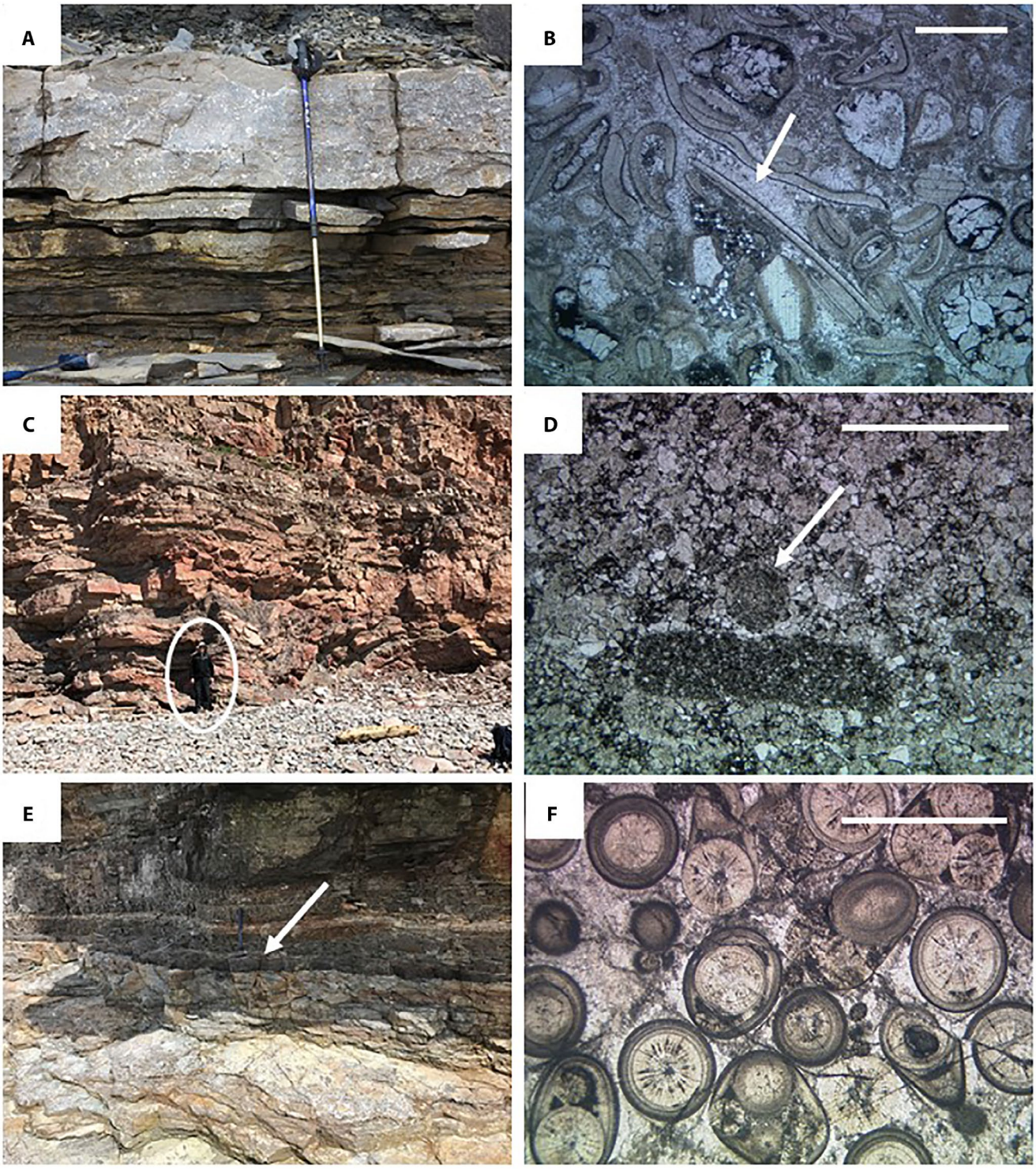

FIGURE 7 Outcrop and thin-section images (scale bars 1000 μm). (A) Big Cove Mbr. (MPS, 167 m). Bioclastic grainstones underlain by ribbon rock. Pole 1 m. (B) Big Cove Mbr. (MPS, 167.25 m). Bioclastic grainstone (trilobite, brachiopod and echinoderm fragments) from base of grainstone shown in (A). Fibrous fringe cements surround grains (arrow). (C) Felix Mbr. (MPS, *ca* 220m). Pink, dolomitised grainstones. Person (circled) for scale. (D) Felix Mbr. (MPS, 213 m). Finely crystalline dolomite with ghost ooid (arrow) and mudstone clast. (E) Man O'War Mbr. (MPS, 230 m). Dark grey oolitic grainstone (arrow) overlying FPC. Hammer, adjacent to arrow, 0.4 m. (F) Man O'War Mbr. (MPS, 231.5 m). Oolitic grainstone with radial, tangential and composite ooids. Fibrous cement fringes surround grains

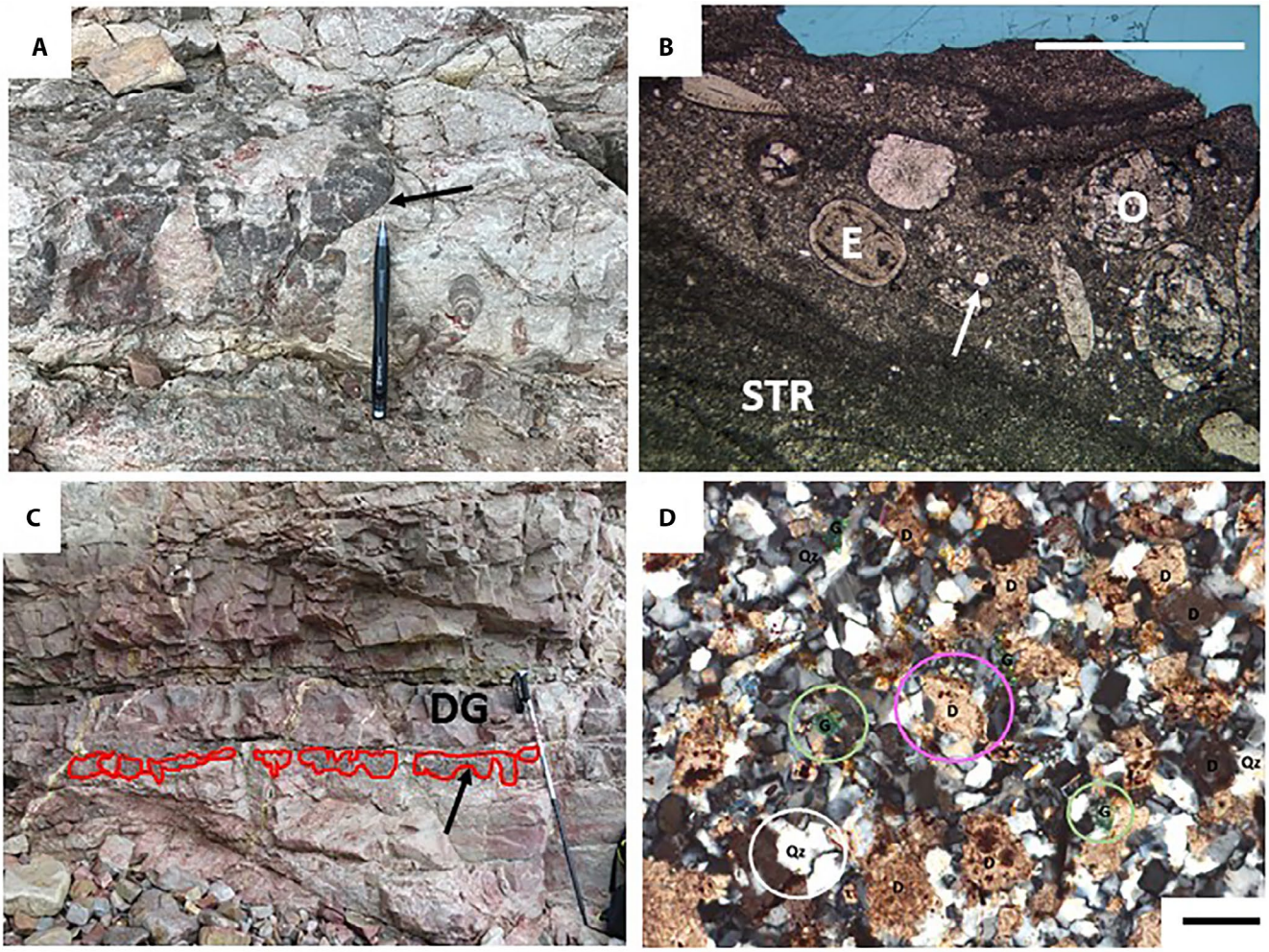

FIGURE 8 MPS outcrop and thin-section images. (A) Felix Mbr. (MPS, 222.25 m). Digitate stromatolite (arrow) at SPICE. (B) Felix Mbr. (MPS, 222.25 m), stromatolite (STR) trapping sediment grains including relict ooids (O), echinoderm and coated echinoderm (E) fragments and fine quartz grains (arrow). Scale bar 1000 μm. (C) Felix Mbr. (MPS, *ca* 222 m). Digitate stromatolite (arrow and outlined in red) at SPICE overlain by dolomitised, glauconitic grainstone (DG). (D) Felix Mbr. (MPS, 225.5 m). Fine dolomitised (D, pink circle) quartz sandstone (Qz, white circle) with glauconite (G, green circle). XP, scale bar 100 μm. 190 × 254 mm (96 × 96 DPI)

coarse, well-rounded quartz grains (Figure 9B,C). In oolitic grainstones, early isopachous fibrous cement fringes and relict oomouldic porosity are observed throughout (Figures 3 and 10B). Radial ooids are less common and observed mainly below the SPICE (Figure 4).

Petit Jardin Formation—Man O'War Member (30 m and above)

A relatively thick layer of ribbon rock from 30 to 35 m marks the base of the Man O'War Member. The top of the Man O'War Member in the measured FCS is not exposed. Thin-section analysis shows the presence of isopachous fibrous cement fringes in oolitic–bioclastic grainstones together with relict oomouldic porosity, partially filled by dolomite (Figure 10A) with only occasional radial ooids (Figure 4).

4.2 | Chemical composition from X-ray fluorescence

In the MPS (Figure 3), dolomitisation (weight percent Ca *ca* 20%) is extensive in the upper part of the PJF (especially the Felix Member). In the FCS, however, dolomitisation is less extensive, with weight % Ca ranging from 20% to 38% (Figure 4). These data are corroborated by petrography, which indicates the most intense dolomitisation in the Felix Member of the MPS (Figures 3, 7D and 8D) compared to the FCS (Figures 4, 9B and 10B).

Layers of shale are clearly identified by increased amounts of Si, Al and Fe in both the MPS and FCS (e.g. MPS 133 m and FCS 21.5 m, Figures 3 and 4). In these shales, Mn levels are low (Figures 3 and 4).

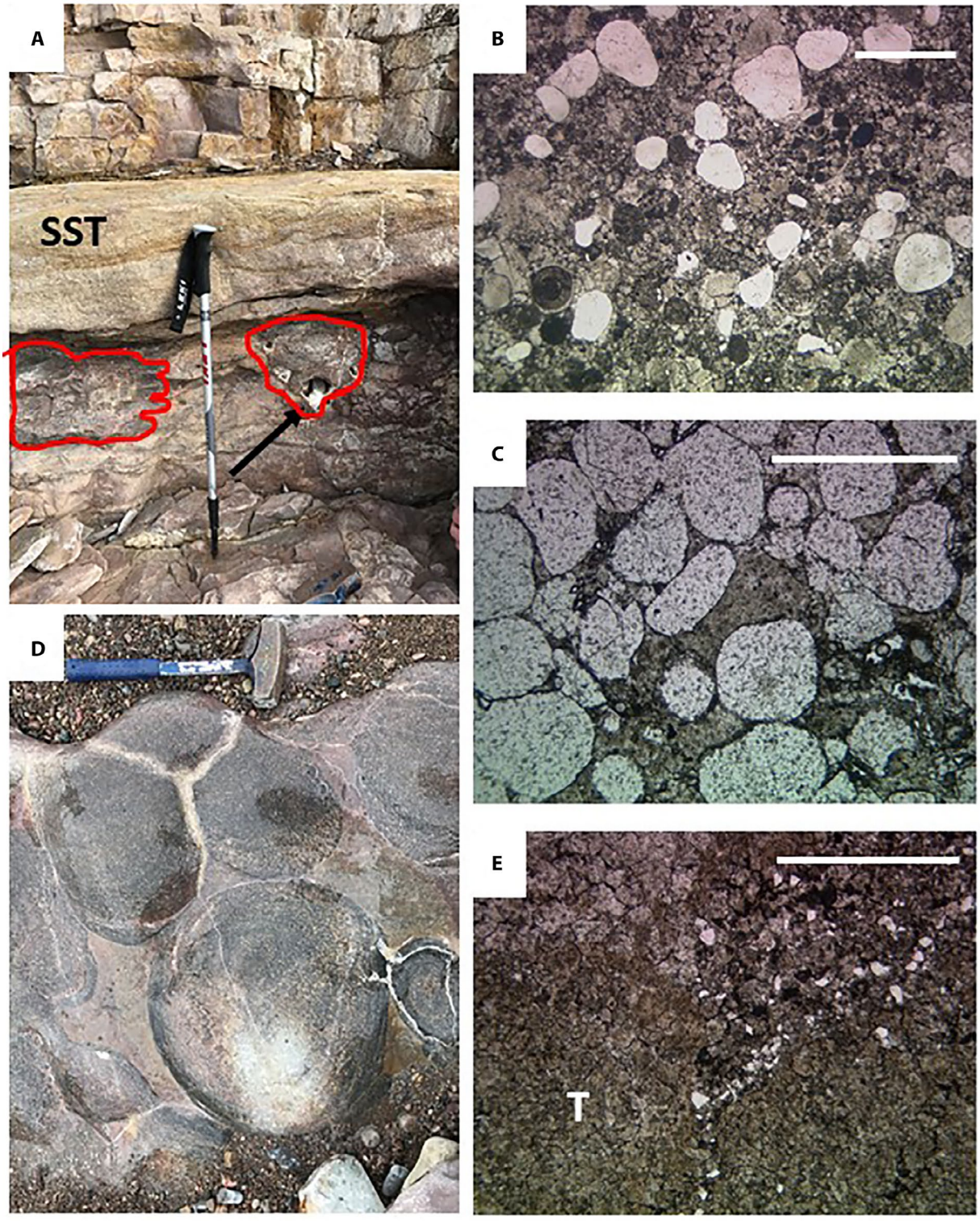

FIGURE 9 FCS SPICE outcrop and thin-section images (scale bars 1000 μm). (A) Felix Mbr. (FCS, 22–23 m). Coarse sandstone (SST) overlying oblate thrombolite layer with calcite cemented vugs (arrow and outlined in red). Pole 0.6 m. (B) Felix Mbr. (FCS, 24 m). Sandy limestone containing coarse, moderately sorted, rounded quartz grains together with oolitic and peloidal grains. (C) Felix Mbr. (FCS, 22.5 m). Coarse, moderately sorted, rounded quartz sandstone with coarse calcite cement. (D) Felix Mbr. (FCS, 22.25 m). Oblate thrombolite which underlies the SPICE sandstone. Hammer 0.4 m. (E) Felix Mbr. (FCS, 22.25 m). Dolomitised thrombolite (T) with fine, sub-rounded to sub-angular quartz grains (white) between clots

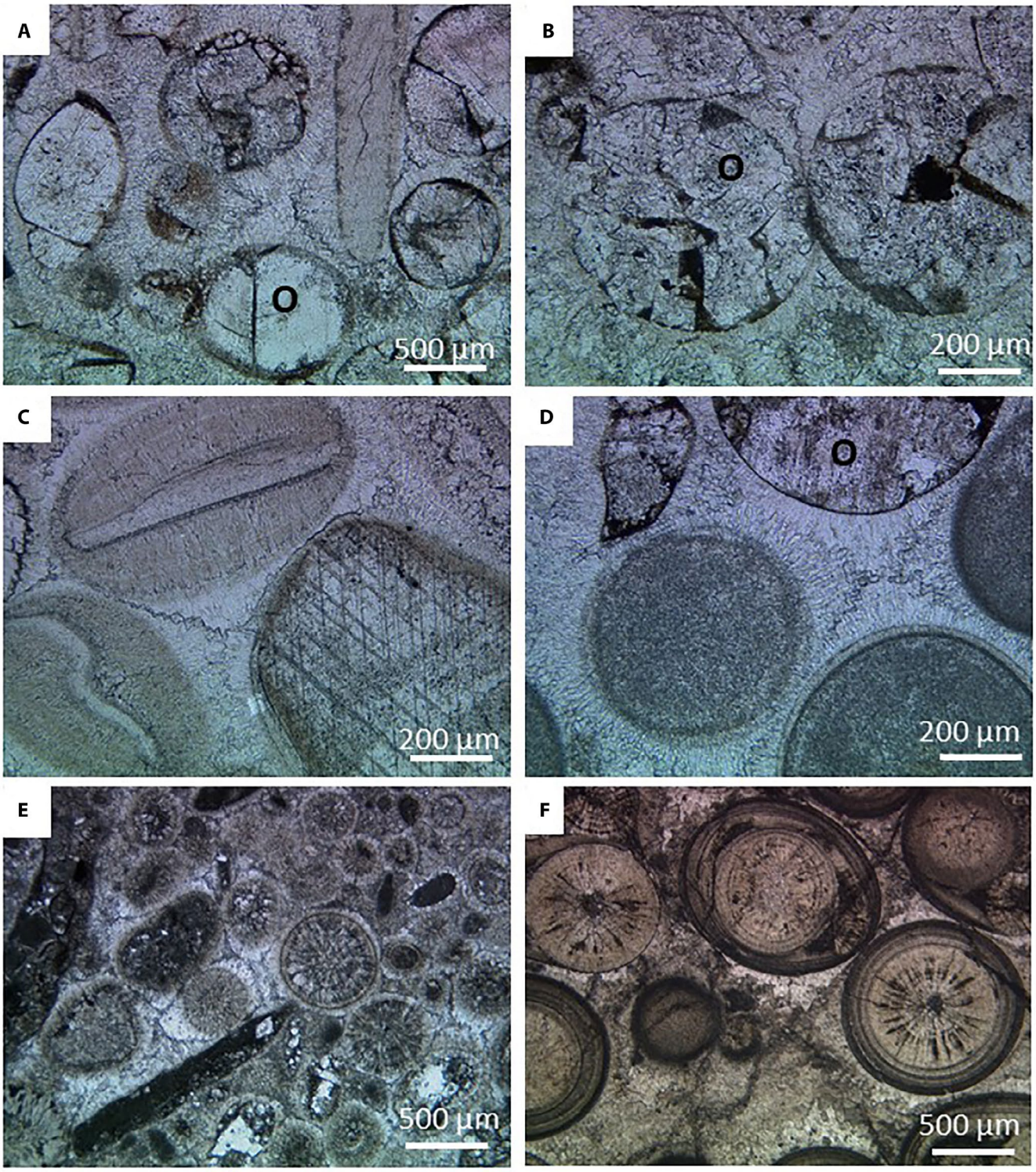

FIGURE 10 Photomicrographs (PPL) of early, fibrous fringe cements in the Port au Port Gp. (A) Man O'War Mbr., FCS (36 m). Oolitic, bioclastic grainstone. Early, fibrous fringes surround relict ooids and bioclasts. Relict oomouldic porosity (O) now filled by dolomite. (B) Felix Mbr., FCS (13 m). Oolitic grainstone. Early, fibrous fringes surround relict ooids and bioclasts. Relict oomouldic porosity (O) now filled by dolomite. (C) Big Cove Mbr., MPS (167.25 m). Oolitic-bioclastic grainstone. Ooids often display bioclastic (brachiopod, trilobite and echinoderm fragments) nuclei. Early fibrous fringes surround grains. (D) Campbells Mbr., MPS (108 m). Oolitic-peloidal grainstone. Early, fibrous fringes surround relict ooids and bioclasts. Relict oomouldic porosity (O) now filled by dolomite. (E) Cape Ann Mbr., MPS (52.4 m). Oolitic-peloidal-bioclastic grainstone. Early, fibrous fringes surround grains. (F) Man O'War Mbr., MPS (231.5 m). Oolitic grainstone. Very well-preserved radial and tangential ooids lacking well-developed fibrous fringe cement. Early cements more prismatic

Several sandy limestones occur in the MPF and PJF but a predominant medium to coarse, well-sorted and rounded, quartz sandstone occurs at 22.5 m in the FCS, coeval with the onset of the positive $\delta^{13}C$ excursion (Figure 4). This sandstone has been cemented by sparry calcite and is high in Mn (1130 ppm, Figure 4). Calcite cement from a vug just above this sample was also found to contain high concentrations of Mn (2056 ppm, Figure 4). The layers immediately below the sandstone at 22.5 m (a thrombolite at 22.25 m and underlying sandstone at 22 m, Figures 4 and 9) also contain high concentrations of Mn (1468 and 1410 ppm respectively). Many of these thrombolite layers (e.g. MPS 223.6 m) contain vugs, which are partially lined by calcite cement (Figure 9A), hence the high amounts of Mn.

Glauconite is most abundant in the lower half of the MPF (Figures 3 and 5B), where it is associated with bioclastic grainstones and sandy limestones. It also occurs in specific layers throughout the PJF in both the MPS and FCS. The pXRF shows that these glauconitic layers typically contain up to 2 wt% Fe but can contain as much as 4.5 wt% (e.g. 9.25 m, MPS, Figure 5B).

Bulk Sr in the MPF and PJF is variable (Figures 3 and 4), with decreased concentrations in dolomitised layers (e.g. MPS 180–270 m, Figure 3). In non-dolomitised members of the PJF, however, Sr increases from the Cape Ann Member at the base (*ca* 200 ppm, Figure 3) to the top of the Big Cove Member (up to 500 ppm, Figure 3). In the relatively non-dolomitised Felix and Man O'War member layers of the FCS, Sr concentrations remain relatively high (up to 600 ppm, Figure 4).

4.3 | Electron microprobe analysis

The Sr and Mg data for the pre-compaction fibrous fringe cements (Figure 10) that surround grains in many of the grainstones in the PJF (Figures 10 and 11) contain up to 7000 ppm Mg (equivalent to 3 mol.% $MgCO_3$) and 5500 ppm Sr (Figure 11A). Other phases (e.g. various grains, intergranular cement and fracture fill cements, Figure 11B) contain less than 1000 ppm Sr, the exception being occasional echinoderm overgrowths (up to 2000 ppm).

Fibrous fringes at the base of the PJF (Cape Ann Mbr.) have low Sr concentrations (average 250 ppm, $n = 8$). Above this, however, the Sr content of the fibrous fringes increases. The overlying Campbells Member has an average Sr content of 604 ppm ($n = 20$), the Big Cove Member an average of 720 ppm ($n = 33$), and the Felix Member having the highest levels (maximum 5500 ppm, average 1136, $n = 47$). Above this in the Man O'War Member, the Sr content of the fibrous fringes decreases slightly (maximum 2500 ppm, average 814, *n* 37).

5 | DISCUSSION

5.1 | Depositional environment of the March Point and Petit Jardin Formations

The units of the PAP, as defined by Chow (1985), Chow and James (1987a) and Cowan and James (1993), fall within three transgressive–regressive sequences ('Grand Cycles'), generated by the relative rate of sea-level rise during the Middle–Late Cambrian (Figure 1). Each Grand Cycle is composed of a lower half shelf cycle consisting of muddy carbonates (ribbon rock *sensu* Cowan & James, 1993) and an upper half shelf cycle of oolitic carbonates (Figure 1).

The lower half cycles consist of the MPF and several members of the PJF (Cape Ann, Big Cove and Man O'War Mbrs). These are characterised by frequently interbedded shales, ribbon rock and FPCs and contain glauconite layers (Figure 5B) and marine bioclasts (Figure 7B). Chow and James (1987a) suggested that these cycles were deposited in intertidal to subtidal environments. However, Cowan and James (1993) observed that ribbon rock in these lower half cycles often coarsens upwards and grades into clean bioclastic and oolitic grainstones, suggesting a shallow subtidal origin (e.g. Figure 7A,F). Cowan and James (1993) also reinterpreted the desiccation cracks reported by Chow and James (1987a, 1987b) as subaqueous diastasis cracks (mechanically generated synaeresis-like cracks generated at or just beneath the sea floor, Cowan & James, 1992). Marine bioclasts are observed in these units (trilobites, echinoderms and brachiopods, e.g. Figure 7B), suggesting relatively open marine conditions, in support of shelf deposition, as suggested by Cowan and James (1993). The ribbon rock and FPC's of the PAP also show many similarities to the Furongian subtidal ribbon rocks in Shandon Province, China (Chen et al., 2010) again supporting the interpretation of the sequence as being subtidal.

Glauconite is also common in these horizons, mainly in the lower part of the MPF (Figure 5B) and in coarser layers within the Big Cove Member (Figure 3). Glauconitic horizons, together with phosphate, were also observed overlying hardgrounds by Chow (1985) and Chow and James (1992) and are interpreted as having formed during sea-floor cementation under low-energy and intermittent sedimentation. In modern marine environments, glauconite forms in relatively deep water at the platform edge, where sedimentation rates are low (Odin, 1988). However, in the Cambrian it was also abundant in shallow-marine shelf waters (Peters & Gaines, 2012). Peters and Gaines (2012) suggest that the increase in the Cambrian was due to unusually high levels of K^+, Fe^{3+} and $H_3SiO_4^-$ flushed into shelf waters, as a result of erosion of the hinterland along the Precambrian–Cambrian 'Great Unconformity'.

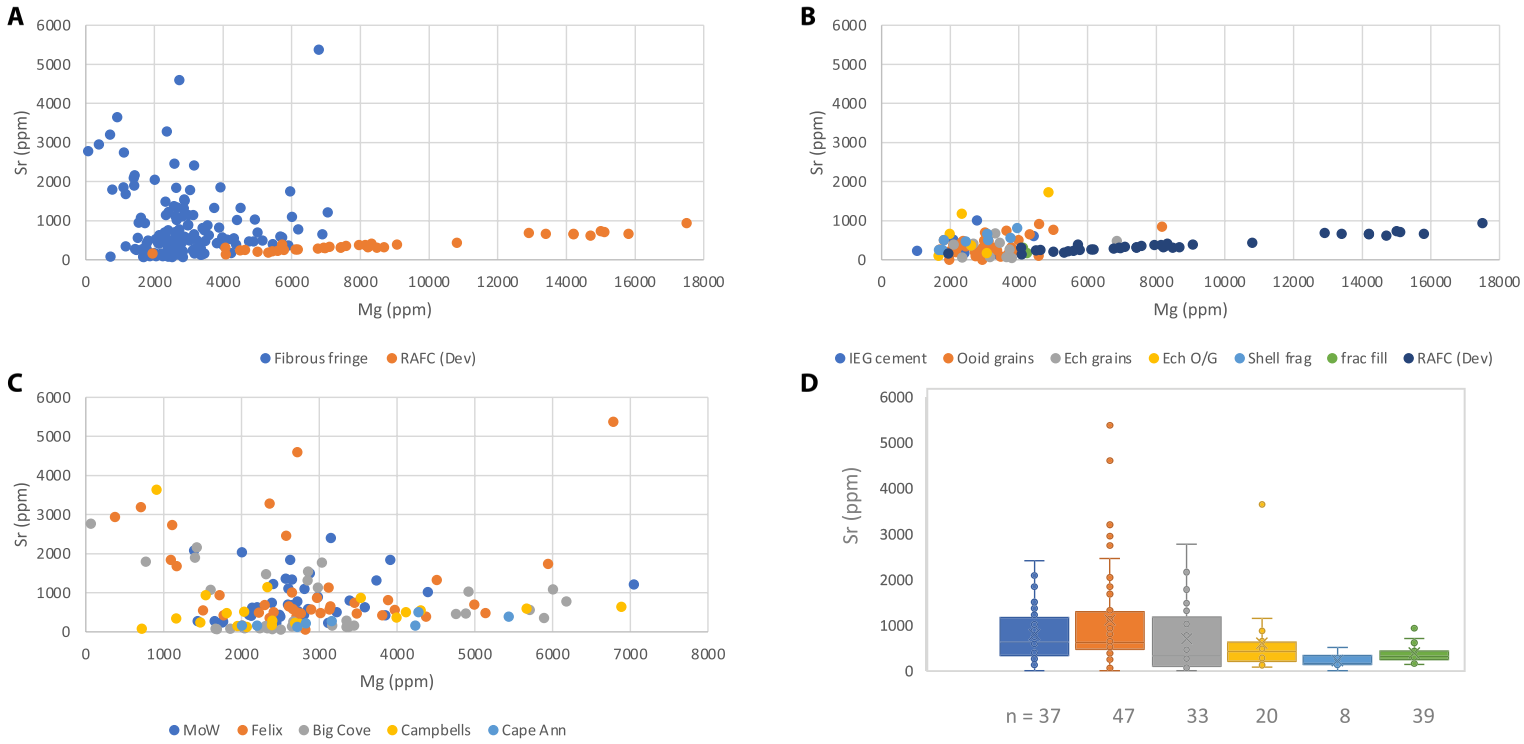

FIGURE 11 Electron microprobe analysis (Sr and Mg ppm) for cements and grains in the Petit Jardin Fm. (PJF) compared to Devonian radial axial cements (Western Canada and Canning basins, Carpenter et al., 1991). (A) PJF fibrous fringe cements compared to Devonian radial axial cements. (B) Grains, intergranular cement and fracture fill cement in the PJ Fm. compared to Devonian radial axial cements. (C) PJF fibrous fringe cements by Member. (D) PJF Box plot fibrous fringe cements by Member (key as in C. Green—Devonian Radiaxial fibrous cements, Carpenter et al., 1991)

Flat pebble conglomerates are another common feature of the PAP lower half cycles. Intraclast pebbles, reworked from PAP hardgrounds are interpreted as having been generated during high energy conditions (Cowan & James, 1993). These layers are frequent in the upper half of the MPF, the Big Cove and Man O' War members and suggest deposition in a subtidal environment. Thin oolitic–intraclastic layers occur in the lower half cycles and commonly contain small radial or composite ooids (Figures 6A,B and 7F). The presence of oolite intraclasts (Figure 6B) may also suggest a degree of storm reworking. Therefore, in the lower half cycles, there is significant evidence of deposition in a subtidal environment as suggested by Cowan and James (1993).

The upper half cycles consist of the Campbells and Felix members of the PJF. These carbonate-rich layers contain oolitic grainstones and microbial deposits, with minor amounts of ribbon rock. These layers correspond to the upper part of the relative transgressive–regressive cycles (Figure 1) of Chow and James (1987a) and the coarsening upwards, oolitic upper half cycles of Cowan and James (1993). Although Chow and James (1987b) identified two types of oolitic grainstone (subtidal grey and intertidal brown oolites), Cowan and James (1993) interpret all of the oolitic grainstones as being subtidal and deposited in the outer part of the shelf.

The oolitic shoal complexes are typically massive, although occasionally exhibit herringbone cross-stratification (Figure 3), as well as low-angle and incipient stratifications, suggesting a tidal, possibly upper subtidal influence. Glauconite is also occasionally found in the upper half cycles (e.g. in the Campbells Member and at the Felix /Man O'War Member boundary), in both the MPS and FCS (Figures 3 and 4). As discussed above, the presence of glauconite in these upper half cycles suggests subtidal deposition (Peters & Gaines, 2012).

The oolitic grains in these shoals are dominantly micritic or relict grains (Figures 6D and 10B through D) in the form of relict oomouldic porosity, often infilled by dolomite rhombs (Figures 3, 4 and 10). Although many authors suggest that mouldic porosity may be an indicator of an originally aragonitic mineralogy (Cantrell, 2006; Ge et al., 2019; Sandberg, 1983; Tucker & Wright, 1990), Sandberg (1983) also suggested that this should only be concluded if accompanied by other evidence for early marine aragonitic precursors (e.g. distinctly higher Sr levels in subsequent replacive calcite). Well-developed, isopachous fibrous cement fringes are observed in clean grainstones throughout the PJF (Figures 3, 4 and 10). These typically formed in the shallow subtidal, marine phreatic environment (Tucker & Wright, 1990).

5.2 | The Steptoean positive carbon isotope excursion

The positive $\delta^{13}C$ SPICE excursion in the PAP, is part of a global phenomenon (Pulsipher et al., 2021; Saltzman et al., 2000). In Newfoundland, it was first identified in the FCS by Saltzman et al. (2004) and in the MPS by Hurtgen et al. (2009). It was subsequently observed in both by Barili et al. (2018) although not as clearly in the MPS as by Hurtgen et al. (2009). Globally, the SPICE $\delta^{13}C$ can reach up to +5 ‰ (Pulsipher et al., 2021; Saltzman et al., 2000) but less so in the PAP. Saltzman et al. (2004) observed a $\delta^{13}C$ excursion of *ca* +3.5‰, Hurtgen et al. (2009) *ca* +4‰, and Barili et al. (2018) *ca* +2.5 to +3‰ (Figures 3 and 4).

A review of published global SPICE data (Pulsipher et al., 2021) confirms that water depth and facies have a significant effect on the extent of the carbon isotope excursion. In the Amadeus Basin (Schmid et al., 2018), open marine sequences were found to show the full +5‰ excursion, whereas nearshore shelf environment deposits displayed a reduced (+2 to +3.5‰) excursion, similar to the values observed in the PAP. According to Schmid et al. (2018), the lower $\delta^{13}C$ signature in nearshore sediments compared to the deep shelf, suggests a possible isotopic gradient between dissolved inorganic carbon in sea water and atmospheric CO_2, which was very high in the Cambrian (3500–4000 μatm, Berner, 2006). Jones et al. (2019) and Pulsipher et al. (2021) suggested that the trend was probably driven by different early diagenetic conditions based on the extent of interaction between sea water and sediment in shallow (fluid-buffered diagenesis) and deep (sediment buffered diagenesis) water carbonates. The thickness of the SPICE also varied in the Amadeus Basin, ranging from 14 to 119 m with thicker sequences in the deeper areas of the basin (Schmidt et al., 2018). The excursion observed in the PAP has a thickness of up to 30 m, comparable to that of a shallow subtidal position in the Amadeus Basin.

Pulsipher et al. (2021) identified three SPICE phases: rising limb, plateau and falling limb. In the MPS, the rising limb is characterised by a digitate stromatolite (222.25 m, Figure 8A,C) overlain by dolomitised grainstones and a fine-grained sandstone (225.5 m, average grain size 38 μm, Table 1, Figure 3) at the top, 3 m above the stromatolite. In the FCS, the rising limb is characterised by fining-up grainstones with a thrombolite (22.25 m, containing fine quartz grains, average grain size 72 μm, Table 1, Figure 4) immediately underlying a prominent coarse-grained sandstone at the top (22.5 m, average grain size 523 μm, Table 1, Figure 9A,C). In a study of microbial structures in the lower Ordovician St Georges Group in Western Newfoundland, Pratt and James (1982) suggested that digitate stromatolites (laminated structures) were deposited in the lower

intertidal to shallow subtidal environment while thrombolites (clotted textures) were entirely subtidal. However, the digitate stromatolite in the MPS, trapped oolitic, coated echinoderm and small amounts of fine quartz grains (average grain size 48 μm, Table 1, Figure 8B) and is directly overlain by a dolomitised, glauconitic grainstone containing fine quartz grains (average grain size 89 μm, Table 1, Figure 8C). It therefore seems probable that the digitate stromatolite grew in the subtidal environment between oolitic shoals as discussed by Cowan and James (1993), similar to the thrombolites in the FCS.

Chow and James (1987a) and James et al. (1989) correlated the sandstone at Felix Cove with the Sauk II–III regression (Figure 1). The coarse, relatively well-sorted and rounded nature of the quartz grains in the FCS suggests original deposition as aeolian sands (Cowan & James, 1993) but the association with glauconite and low-angle cross-bedding suggests reworking and deposition in the subtidal, shoreface environment (Tucker & Wright, 1990). The different character of the microbial structures at the two localities, oblate thrombolites in the FCS, and digitate stromatolites in the MPS, together with the different characteristics of the quartz grains, suggest deposition in slightly different positions on the shelf albeit in a shallow subtidal environment.

Following deposition of sandstone at the end of the rising limb of the SPICE, the SPICE plateau (Pulsipher et al., 2021) is characterised by coarse-grained sandy limestones in the FCS. At 23, 23.4 and 24 m, average quartz grain size is 473, 466 and 473 μm respectively ($n = 31$ in each, Table 1 and Figure 9B). No thin-sections are available for plateau samples in the MPS but in both sections, the falling limb is characterised by ribbon rock with interbedded oolitic grainstones (Figures 3 and 4).

Saltzman et al. (2004) indicate that the rising limb and plateau occur in the Felix Member (FCS) and the falling limb occurs in the Man O'War Member, while Hurtgen et al. (2009) suggests that the Man O'War Member contains part of the plateau and falling limb (MPS). However, neither study present a detailed lithological description. This study shows that the depositional environment during the SPICE varied slightly between the MPS and FCS and that a direct lithostratigraphic correlation is not possible. It is suggested however that, despite having different characteristics, the sandstone at the top of the rising SPICE limb in both the MPS and FCS marks the point of maximum regression and can be regarded as a potential regional marker.

The effect of diagenesis on the isotopic signature is a matter of concern in ancient rocks. In limestones, meteoric diagenesis can reduce both $\delta^{18}O$ and $\delta^{13}C$ signatures, due to the depleted isotopic content of freshwater and interaction with photosynthesising communities respectively (Knauth & Kennedy, 2009; Land, 1986). Burial diagenesis and interaction with burial fluids rich in oxygen also leads to a negative shift in $\delta^{18}O$ due to increasing temperature and consequential oxygen isotope fractionation (Machel & Buschkuehle, 2008; Tucker & Wright, 1990) but carbon isotopes are less affected (Banner & Hanson, 1990; Knauth & Kennedy, 2009), especially in platform interiors where the $\delta^{13}C$ sedimentary signatures tend to be preserved (Hoffman & Lamothe, 2019).

Petrography and pXRF data show the Felix and Man O'War members in the MPS (Figure 3) were more affected by dolomitisation (Ca *ca* 20%) compared to the FCS (Figure 4). The $\delta^{13}C$ trend in the FCS is similar in Saltzman et al. (2004) and Barili et al. (2018) but in the MPS the $\delta^{13}C$ signature in Hurtgen et al. (2009) is much clearer than in Barili et al. (2018). In the latter study, the rising limb is clear but the plateau and falling limbs are absent. Dolomitisation can have an effect but while the $\delta^{18}O$ signature is controlled by pore fluid temperature, $\delta^{13}C$ is strongly influenced by the composition of the carbonate precursor as burial pore fluids are low in carbon and there is little carbon isotopic fractionation with temperature (Hoefs, 2018; Tucker & Wright, 1990). Since dolomite $\delta^{13}C$ is normally similar to

TABLE 1 Quartz grain size for MPS and FCS (modified after Barili et al., 2018)

Section	Height (m)	Average (μm)	Maximum (μm)	Minimum (μm)	Median (μm)	*n*
MPS	222.60	35	80	18	34	33
MPS	222.5	89	224	36	78	31
MPS	222.3	88	338	37	75	31
MPS	222.25	45	89	22	44	28
MPS	218.75	68	100	51	60	4
FCS	24	456	858	138	409	31
FCS	23.4	466	815	227	439	31
FCS	23	473	734	116	504	31
FCS	22.5	523	933	265	496	40
FCS	22.25	72	195	29	60	77

MPS stromatolite at 222.25 m, FCS thrombolite at 22.25 m (both highlighted in green).

the original signature and the rising limb is observed in both data sets, it is not thought that dolomitisation was the cause of the variation between the two data sets. The reasons are unclear but it may possibly be due to differences in sampling and/or analytical techniques.

Manganese concentrations also increase at the SPICE (Figures 3 and 4) within the calcite cements associated with sandstone and vuggy porosity in microbial structures (Figure 9A,C). Reducing conditions favours the presence of Mn in pore fluids (Tucker & Wright, 1990), with high Mn often found in carbonates significantly affected by burial diagenesis (Derry, 2010). In the clean, sparry calcite cemented SPICE sandstone in the FCS at 22.5 m, $\delta^{18}O$ values of −9‰ and high Mn suggest elevated calcite precipitation temperatures (Figure 4). In the dolomitised layers of the MPS, however, Mn is generally low (Figure 3) suggesting that burial resetting of the dolomites did not occur.

5.3 | Evidence for precipitation of inorganic aragonite on the lead up to and around the SPICE

Understanding the chemistry and conditions of sea water at the time is critical, especially considering a major extinction occurred at the SPICE (Zhuravlev & Wood, 2018). Together with the bulk chemistry, investigation of the early marine cements that precipitated from sea water soon after sediment deposition, can help elucidate the sea water chemistry and conditions during this time.

The concept of aragonite and calcite seas is well-documented and major secular changes in mineralogy largely occur in response to variations in Mg/Ca ratios, related to plate tectonic activity and oceanic spreading (Hardie, 1996; Lowenstein et al., 2001). While Mg/Ca ratios >2 favour the precipitation of inorganic aragonite, Mg/Ca ratios <2 favour the inorganic precipitation of calcite (Balthasar & Cusack, 2015; Füchtbauer & Hardie, 1976; Ries, 2009). Temperature and pCO_2 also affect $CaCO_3$ mineralogy (Balthasar & Cusack, 2015; Burton & Walter, 1987; Lee & Morse, 2010; Sandberg, 1983). The rate of transition between aragonite and calcite seas is also poorly resolved (Vulpius & Kiessling, 2018) and the distinction can be 'fuzzy' (Kiessling, 2015).

Cambrian Series 3 (Middle Cambrian) and the Furongian (Late Cambrian) are generally believed to have had Mg/Ca ratios <0.8, suggesting early LMC marine cements (Stanley et al., 2010). Various studies however suggest that the Mg/Ca ratio in the Middle–Late Cambrian could have been 1.2 (Arvidson et al., 2006) or 1.6–2 (Horita et al., 2002). Experimental work by Balthasar and Cussack (2015) also suggests that a combination of Mg/Ca ratios of around 1.2, pCO_2 values above 2500 μatm (Lee & Morse, 2010) and warm tropical waters, can promote the precipitation of inorganic aragonite.

Fibrous marine cements and relict oomouldic porosity have previously been shown to have precipitated around the time of the SPICE in the Al Bashair Formation, Andam Group, Oman (Neilson et al., 2016) with cements containing up to 1000 ppm Sr. Sandberg (1983) and more recently Jones et al. (2019), suggest that an elevated Sr content suggests an aragonitic precursor. Pederson et al. (2019) also showed during experimental studies that Sr signatures can be retained in calcite that has replaced aragonite during neomorphism. Neilson et al. (2016) concluded that the fibrous cements in the Al Bashir Formation originally precipitated as aragonite or HMC which can also contain elevated levels of Sr (Carpenter et al., 1991).

Radial ooids (suggesting a calcite precursor) occur in varying degrees throughout the PJF (Figures 3 and 4). Relict oomouldic porosity (suggesting an aragonite precursor) is also observed but is most abundant in the upper half cycles, particularly towards the ends of the Grand Cycles (Figure 1) which would have been accompanied by regression (Chow & James, 1987a). Land et al. (1979) suggested that the aragonitic ooids of Baffin Bay formed in areas of maximum agitation, fitting with shallower water environments towards the end of the Grand Cycles. Relict oomouldic porosity is also often associated with microbial buildups in the PAP (Figures 3 and 4). Rao and Gopinathan (2019) suggest that aragonite ooids can be the result of calcification of microbial filaments. Microbialites are commonly found in the aftermath of mass extinctions and the abundance is related to atmospheric composition and sea water chemistry (Riding, 2011). They were particularly common when pCO_2 was more than 10 times present atmospheric levels (e.g. late Cambrian, Riding, 2006) and when sea water temperature was rising. Both of these factors would have increased the carbonate saturation state of sea water, stimulating microbial calcification (Riding, 2006) and the generation of aragonitic ooids.

In the PJF, early fibrous marine cements increase in abundance towards the SPICE after which they decrease (Figures 3 and 4). These contain variable amounts of Sr, up to 5500 ppm (Figure 11A). The Sr content increases upwards from a few hundred ppm in the Cape Ann Member, to maximums of 1000 ppm in the Campbells Member, *ca* 3000 ppm in the Big Cove Member and 5500 ppm in the Felix Member before dropping to a maximum of 2500 ppm in the Man O'War Member (Figure 11C,D). The microprobe data were compared with relict Devonian HMC cements from the Western Canada Basin (Figure 11A, data from Carpenter et al., 1991). The Mg and Sr contents of the Devonian HMC cements are comparable to those of the Cape Ann Member (Figure 11C,D). However, most of the fibrous cements from the overlying members of the PJF (Figure 11D) have

significantly higher Sr content compared to the Devonian cements, suggesting that the fibrous marine cements precipitated in layers above the Cape Ann Member were probably originally composed of aragonite rather than HMC.

If the fibrous cements were indeed originally precipitated as aragonite, the issue arises as to why they did not undergo dissolution in the same manner as the ooids. Possible reasons for this include (a) variations in the amount of organic matter associated with ooids and fibrous cements and (b) differences in structural characteristics of the phases. Experimental studies by Pederson et al. (2020) have shown that different types of aragonite (crystals, speleothems, bivalves and corals) undergo diagenesis at different rates and via different pathways depending on the amount of associated organic matter and variations in factors such as porosity and permeability within individual grains).

Diaz et al. (2015) have shown that the processes of ooid formation can result in significant amounts of both intercrystalline and intracrystalline organic matter. Aragonite crystals on the other hand contain very little (Pederson et al., 2020). In oxidising environments (e.g. surface or shallow burial), the decomposition of organic matter through processes such as sulphate oxidation or nitrification, can result in dissolution of $CaCO_3$ (Diaz et al., 2015; Laya et al., 2021). It is unlikely that the PJF would have been affected by fluids rich in oxygen during its early diagenesis. However, during burial, the organic matter within the ooids could have generated CO_2 through thermal decomposition (Giles & Marshall, 1986). This could then have combined with organic bound water, also released during organic matter decomposition (Pederson et al., 2019), to form carbonic acid capable of dissolving the aragonite within the grains in a semi-closed diagenetic system.

Differences in the size of aragonite crystals in the fibrous cements and ooids could also have had an effect. Smaller crystals and higher porosity within the ooids would have increased the surface area to volume ratio, leading to higher rock–fluid interaction and increasing dissolution rates (Briese et al., 2017; Jonas et al., 2017; Pederson et al., 2020). Diagenesis in the low porosity, organic poor, fibrous cements would have been rock–buffered (resulting in limited alteration) while diagenesis in the more porous, relatively organic-rich ooids would have been fluid–buffered, causing dissolution and the formation of oomoulds. The study by Pederson et al. (2020) shows that different carbonate phases in one sample can undergo very different diagenetic pathways.

Another reason for difference in preservation between the fibrous cements and ooids is that the fibrous cements may have originally been composed of HMC rather than aragonite. In a study of Holocene abiotic HMC cements, however, Carpenter and Lohman (1992) reported Sr concentrations from 200 to 1900 ppm, less than the maximum observed in the Felix Member (5500 ppm Sr). It is therefore difficult to be definitive as to whether the fibrous cements were originally composed of aragonite or HMC but the elevated Sr contents, along with the precipitation of coeval aragonite ooids would suggest that they most probably were aragonitic. What is clear is that the early fibrous cements are unlikely to have been composed of LMC. In the PJF, analysis of post-dating intergranular calcite cements and fracture fill calcite shows significantly less Sr or Mg than either the PJF or Devonian fibrous marine fringe cements (Figure 11B), suggesting that non-fibrous cements were precipitated as LMC but not the earlier fibrous cements as would have been expected during the 'calcite seas' of the late Cambrian.

5.4 | Relationship of mineralogy to positive carbon isotope excursions

Enhanced burial and preservation of organic matter would have occurred during the SPICE, creating an increase in $\delta^{13}C$ values (Hurtgen et al., 2009; Saltzman et al., 2000). Processes such as these are common during times of warmer seas, reduced thermohaline circulation and anoxia (Hurtgen et al. 2009; Mackenzie et al., 2000). As discussed by Neilson et al. (2016), aragonite could have precipitated on the lead up to and during the SPICE due to warm sea waters, Mg/Ca ratios of 1.2–2 (Arvidson et al., 2006; Horita et al., 2002) and high pCO_2, as would have been the case in the Cambrian (Berner, 2006). Evidence of relict aragonite ooids is observed globally at this time (Conley, 1977; Martin et al., 1980; Neilson et al., 2016). Similarities also exist when comparing the carbonates of the PJF (this study) and the Al Bashar Formation (Neilson et al., 2016) to other periods of positive carbon isotope excursions (CIEs), such as the Upper Ordovician CIE and the Triassic–Jurassic boundary.

During the Upper Ordovician Hirnantian isotopic carbon excursion (HICE), there is evidence of aragonite precipitation during a time of 'calcitic seas' (Jones et al., 2019; Kimmig & Holmden, 2017). In a study of the HICE (<1.3 Myr duration) in Anticosti Island (Canada) and the Great Basin (Nevada and Utah, USA), Jones et al. (2019) suggested that elevated Sr/Ca ratios at the time are consistent with aragonitic precursor sediments. Jones et al. (2019) suggest that low-latitude shallow platforms were warm and able to precipitate aragonite as suggested by Balthasar and Cusack (2015), even during the associated glaciation and suggest that the high Sr/Ca, elevated $\delta^{13}C$ values (+1 to +4‰) and low $\delta^{44}Ca$ was a result of sediment buffered early marine diagenesis.

As at the SPICE, significant environmental change and faunal extinction occurred immediately prior to

the positive CIE at the base of the Jurassic in the Ghalia Formation, United Arab Emirates (Ge et al., 2018) and the Trento Platform in the Lombardy Basin, Italy (Jost et al., 2017; Vulpius & Kiessling, 2018). This positive CIE is also accompanied by an increase in bulk Sr (up to 2000 ppm in the UAE, Ge et al., 2018 and 3000 ppm in Italy, Jost et al., 2017). In the Ghalilah Formation (UAE, Ge et al., 2018), the sedimentological patterns are very similar to those observed in the PJF (this study) and the Al Bashir Formation (Neilson et al., 2016). In the Ghalilah Formation, Late Triassic (Rhaetian) bioclastic limestones (Sumra Mbr.) deposited in 'aragonite seas' are overlain by Early Jurassic (Hetangian) oolitic limestones of the Sakhra Member deposited in 'calcite seas'. These are interbedded with microbialites and wind-blown clastics and display relict oomouldic porosity. In a study of the equivalent Triassic–Jurassic boundary in the Trento Platform (Lombardy Basin, Italy), Vulpius and Kiessling (2018) suggested that Hettangian and Sinemurian (earliest Jurassic), ooids that display relict oomouldic porosity were probably primarily aragonitic, whilst later Pliensbachian and Toarcian very well-preserved, ooids were primarily composed of calcite. This original inorganic aragonitic mineralogy is also seen in the PJF, in the form of relict oomouldic porosity and early Sr-rich fibrous marine cements (Figure 10). As in the Trento Platform, well-preserved ooids post-date the SPICE in the Man O'War Member of the PJF (Figures 7F and 10F) signalling a return to primary calcite precipitation. Time equivalent to the pronounced CIE recorded in the oolites of the early Jurassic Sakhra Member (Galilah Fm.), an increase in bulk Sr (up to 2000 ppm) was observed by Ge et al., (2018). Ge et al. (2018) suggested that the Sr increase was caused by extinction of the mainly aragonitic secreting fauna at the end of the Triassic, increasing sea water Sr concentrations and continental weathering. Jost et al. (2017), however, suggest that the increase in Sr, which is also observed in the Lombardy Basin, Italy (up to 3000 ppm, Jost et al., 2017), came from locally abundant aragonite.

The early Jurassic CIE is ultimately attributed to a large injection of CO_2 and climate warming due to the Central Atlantic Magmatic Province (CAMP) volcanism (Ge et al., 2018; Jost et al., 2017). It is believed that CAMP-related climate and ocean warming would have increased primary productivity and promoted oceanic anoxia (Richoz et al., 2012), resulting in the positive CIE. Increased pCO_2 and warm oceanic conditions has therefore been associated with the precipitation of inorganic aragonite as ooids, early marine cements and increased Sr concentrations at various global locations through time. At the Triassic–Jurassic boundary, which marks the last major shift from aragonite to calcite seas (Vulpius & Kiessling, 2018), precipitation of inorganic aragonitic ooids continued into the early Jurassic (calcite seas), up to the Pliensbachian over a period of 10 Myr. The transition between aragonite to calcite seas and vice-versa, is poorly constrained.

The implications of the current study are that either (i) a period of 'aragonite seas', at least regionally, occurred in the Late Cambrian (Furongian) driven by the processes responsible for the development of the SPICE, that is warm ocean waters and high pCO_2 or (ii) the inorganic precipitation of early marine aragonite cements and ooids in the Late Cambrian (Furongian) were purely local events. The global distribution of relict early marine fibrous cements rich in Sr and relict oomouldic porosity (hence interpreted as aragonitic ooids) suggests more than a local phenomenon. Significant uncertainties exist as to sea water Mg/Ca ratios at the time (estimates vary from 0.8 to 2) which warrants further investigation.

6 | CONCLUSIONS

1. This study presents new petrographic and geochemical data from the subtidal, shallow Port au Port Group shelf (PAP, Middle–Late Cambrian) in Western Newfoundland. During deposition of the PAP, analysis shows that aragonite was precipitated in the form of ooids and, early marine fibrous cements during a time of stable 'calcite seas'.
2. Aragonitic ooids, accompanied by increased microbial production, were largely formed towards the end of the Sauk Grand Cycles during relative sea-level regression. The rising limb of the SPICE at the end of Sauk II, is marked by a sedimentary package containing microbialites (thrombolites and stromatolites) and fine-to-coarse-grained sandstones cemented by calcite.
3. Early fibrous marine cements occur throughout the PJF of the PAP, with Sr concentrations increasing upward towards the SPICE to a maximum of 5500 ppm after which their abundance and Sr content decreases.
4. The precipitation of inorganic aragonite on the lead up to the SPICE was probably controlled by warm ocean water and high pCO_2, factors also favouring microbialite formation.
5. Similarities exist with other positive CIEs. During a time of 'calcite seas', aragonite precursors are suggested by elevated Sr/Ca ratios in the Upper Ordovician HICE (<1.4 Myr). The Triassic–Jurassic CIE is marked by an increase in sea water Sr and deposition of aragonitic ooids post-dating the shift from 'aragonite to calcite seas' by *ca* 10 Myr.
6. The precipitation of inorganic aragonite during 'calcite seas' at the SPICE, the HICE and the Triassic–Jurassic positive CIE may have been controlled by the same factors, that is warm ocean water and high pCO_2, at least on a regional scale.

ACKNOWLEDGEMENTS

The authors would like to thank the following bodies for funding this research: Shell Brazil through the 'BG05: UoA-UFRGS_SWB Sedimentary Systems' project at UFRGS, the Aberdeen Formation Evaluation Society and the University of Aberdeen. LAMIR, BGS and EPMA staff are also thanked for their assistance with stable isotope and electron microprobe analysis. Dr Ilse Kamerling and Dr. D. Kemp are thanked for their assistance with pXRF analysis, Marianna Skupinska with collection of point count data and Prof. D. McIlroy is thanked for his assistance during fieldwork. Reviews by Dr C. Pederson, Prof. P. Swart and two anonymous reviewers helped improve the manuscript significantly.

DATA AVAILABILTY STATEMENT

The data that support the findings of this study are available from the corresponding author upon reasonable request.

ORCID

Joyce E. Neilson https://orcid.org/0000-0001-6213-2373

REFERENCES

Arvidson, R.S., Mackenzie, F.Y. & Guidry, M. (2006) MAGic: a Phanerozoic model for the geochemical cycling of major rock-forming components. *American Journal of Science*, *306*, 135–190. https://doi.org/10.2475/05.2007.04

Balthasar, U. & Cussack, M. (2015) Aragonite-calcite seas – quantifying the gray area. *Geology*, *43*, 99–102. https://doi.org/10.1130/G36293.1.

Banner, J.L. & Hanson, G.N. 1990. Calculation of simultaneous isotopic and trace element variations during water-rock interaction with applications to carbonate diagenesis. *Geochimica et Cosmochimica Acta 54*, 3123–3137.

Barili, R., Neilson, J.E., Brasier, A.T., Goldberg, K., Pastro Bardola, T., De Ros, L.F. & Leng, M. (2018) Carbon isotopes, stratigraphy, and environmental change: the Middle-Upper Cambrian Positive Excursion (SPICE) in Port au Port Group, western Newfoundland. *Canadian Journal of Earth Sciences*, *55*, 1209–1222. https://doi.org/10.1139/cjes-2018-0025

Berner, R.A. (2006) GEOCARBSULF: a combined model for phanerozoic atmospheric O_2 and CO_2. *Geochimica et Cosmochimica Acta*, *70*, 5653–5664. https://doi.org/10.1016/j.gca.2005.11.032

Briese, L., Arvidson, R.S. & Luttge, A. (2017) The effect of crystal size variation on the rate of dissolution – a kinetic Monte Carlo study. *Geochimica et Cosmochimica Acta*, *212*, 167–175. https://doi.org/10.1016/j.gca.2017.06.010

Burton, E.A. & Walter, L.M. (1987) Related precipitation rates of aragonite and Mg calcite from seawater – temperature or carbonate ion control? *Geology*, *15*, 111–114.

Cantrell, D.L. (2006) Cortical fabrics of Upper Jurassic ooids, Arab Formation, Saudi Arabia: implications for original carbonate mineralogy. *Sedimentary Geology*, *186*, 157–170. https://doi.org/10.1016/j.sedgeo.2005.11.015

Carpenter, S.J., Lohman, K.C., Holden, P., Walter, L.M., Huston, T.J. & Halliday, A.N. (1991) $\delta^{18}O$ values, $^{87}Sr/^{86}Sr$ and Sr/Mg ratios of Late Devonian abiotic marine calcite: implications for the composition of ancient seawater. *Geochimica et Cosmochimica Acta*, *55*, 1991–2010.

Carpenter, S.J. & Lohmann, K.C. (1992) Sr /Mg ratios of modern marine calcite: empirical indicators of ocean chemistry and precipitation rate. *Geochimica et Cosmochimica Acta*, *56*, 1837–1849.

Chen, J.T., Han, A.Z., Zhang, X.L., Fan, A.P. & Yang, R.C. (2010) Early diagenetic deformation structures of the Furongian ribbon rocks in Shandong Province of China—a new perspective of the genesis of limestone conglomerates. *Science China Earth Sciences*, *53*, 241–252. https://doi.org/10.1007/s11430-010-0010-6

Chow, N. (1985) Sedimentology and diagenesis of Middle and Upper Cambrian platform carbonates and siliciclastics, Port au Port Peninsula, western Newfoundland. Unpublished thesis, 458.

Chow, N. & James, N.P. (1987a) Cambrian grand cycles: a northern Appalachian perspective. *Geological Society of America Bulletin*, *98*, 418–429. https://doi.org/10.1130/0016-7606(1987)98<418

Chow, N. & James, N.P. (1987b) Facies specific, calcitic and bimineralic ooids from Middle and Upper Cambrian platform carbonates, Western Newfoundland, Canada. *Journal of Sedimentary Petrology*, *57*, 907–921.

Chow, N. & James, N.P. (1992) Synsedimentary diagenesis of Cambrian peritidal carbonates: evidence from hardgrounds and surface paleokarst in the Port au Port Group, western Newfoundland. *Bulletin of Canadian Petroleum Geology*, *40*, 115–127.

Conley, C.D. (1977) Origin of distorted ooliths and pisoliths. *Journal of Sedimentary Petrology*, *47*, 554–564. https://doi.org/10.1306/212F71DF-2B24-11D7-8648000102C1865D

Cowan, C.A. & James, N.P. (1992) Diastasis cracks: mechanically generated synaeiesis-like cracks in Upper Cambrian shallow water oolite and ribbon carbonates. *Sedimentology*, *39*, 1101–1118. https://doi.org/10.1111/j.1365-3091.1992.tb01999.x

Cowan, C.A. & James, N.P. (1993) The interactions of sea-level change, terrigenous-sediment influx, and carbonate productivity as controls on Upper Cambrian Grand Cycles of western Newfoundland Canada. *Geological Society of America Bulletin*, *105*, 1576–1590. https://doi.org/10.1130/0016-7606(1993)105<1576:TIOSLC>2.3.CO;2

Cunha, R.B. (2019) Sedimentologia, Petrologia e Geoquímica Do Grupo Port Au Port (Cambriano) em Terra Nova (Newfoundland), Canadá. Universidade Federal do Rio Grande do Sul, Brazil, Thesis, 177 p. http://hdl.handle.net/10183/204830

Derry, L.A. (2010) A burial diagenesis origin for the Ediacaran Shuram-Wonokacarbon isotope anomaly. *Earth and Planetary Science Letters*, *294*, 152–162. https://doi.org/10.1016/j.epsl.2010.03.022

Diaz, M.R., Swart, P.K., Eberli, G.P., Oehlert, A.M., Devlin, Q., Saeid, A. & Altabet, M.A. (2015) Geochemical evidence of microbial activity within ooids. *Sedimentology*, *62*, 2090–2112. https://doi.org/10.1111/sed.12218.

Dickson, J.A.D. (1965) A modified staining technique for carbonates in thin-section. *Nature*, *205*, 587. https://doi.org/10.1038/205587a0.

Füchtbauer, H. & Hardie, L.A. (1976) Experimentally determined homogeneous distribution coefficients for precipitated magnesian calcites: application to marine carbonate cements. *Geological Society of America Abstracts Programme*, *8*, 877.

Ge, Y., Al-Suwaidi, A.H., Shi, M., Li, Q., Morad, S. & Steuber, T. (2019) Short-term variation of ooid mineralogy in the Triassic-Jurassic boundary interval and its environmental implications: evidence from the equatorial Ghalilah Formation, United Arab Emirates. *Global and Planetary Change*, *182*, 103006–103021. https://doi.org/10.1016/j.gloplacha.2019.103006.

Ge, Y.Z., Shi, M., Steuber, T., Al-Suwaidi, A.H. & Suarez, M.B. (2018) Environmental change during the Triassic-Jurassic boundary interval of an equatorial carbonate platform: sedimentology and chemostratigraphy of the Ghalilah Formation, United Arab Emirates. *Palaeogeography, Palaeoclimatology, Palaeoecology*, *502*, 86–103. https://doi.org/10.1016/j.palaeo.2018.04.026

Giles, M.R. & Marshall, J.D. (1986) Constraints on the development of secondary porosity in the subsurface: re-evaluation of processes. *Marine and Petroleum Geology*, *3*, 243–255.

Hall, G.E.M., Bonham-Carter, G.F. & Buchar, A. (2014) Evaluation of portable X-ray fluorescence (pXRF) in exploration and mining: phase 1, control reference materials. *Geochemistry: Exploration Environment, Analysis*, *14*, 99–123. https://doi.org/10.1144/geochem2013-241

Hardie, L.A. (1996) Secular variation in seawater chemistry: an explanation for the coupled secular variation in the mineralogies of marine limestones and potash evaporites over the past 600 my. *Geology*, *24*, 279–283. https://doi.org/10.1130/0091-7613(1996)024<0279:SVISCA>2.3.CO;2

Hoefs, J. (2018) Variations of stable isotope ratios in nature. In: *Stable isotope geochemistry*, 8th edition. Switzerland: Springer, pp. 1–433. https://doi.org/10.1007/978-3-662-02290-0.

Hoffman, P.F. & Lamothe, K.G. (2019) Seawater-buffered diagenesis, destruction of carbon isotope excursions and the composition of DIC in Neoptroterozoic oceans. *Proceedings of the National Academy of Sciences*, *116*, 18874–18879. https://doi.org/10.1073/pnas.1909570116.

Horita, J., Zimmermann, H. & Holland, H.D. (2002) Chemical evolution of seawater during the Phanerozoic: implications from the record of marine evaporites. *Geochimica et Cosmochimica Acta*, *66*, 3733–3756. https://doi.org/10.1016/S0016-7037(01)00884-5

Hurtgen, M.T., Pruss, S.B. & Knoll, A.H. (2009) Evaluating the relationship between the carbon and sulfur cycles in the later Cambrian ocean: an example from the Port au Port Group, western Newfoundland, Canada. *Earth and Planetary Science Letters*, *281*, 288–297. https://doi.org/10.1016/j.epsl.2009.02.033

James, N.P., Stevens, R.K., Barnes, C.R. & Knight, I. (1989) Evolution of a lower Paleozoic continental-margin carbonate platform, Northern Canadian Appalachians. In: Crevello, P.D., Wilson, J.L., Sarg, J.F. & Read, J.F. (Eds.) *Controls on carbonate platforms and basin development*. *SEPM Society for Sedimentary Geology*. Special Publication. Vol. *44*, pp. 123–146. https://doi.org/10.2110/pec.89.44.0123

Jonas, L., Müller, T., Dohmen, R., Immenhauser, A. & Putlitz, B. (2017) Hydrothermal replacement of biogenic and abiogenic aragonite by Mg-carbonates–relation between textural control on effective element fluxes and resulting carbonate phase. *Geochimica et Cosmochimica Acta*, *196*, 289–306.

Jones, D.S., Brothers, W.R., Crüger Ahm, A.S., Slater, N., Higgins, J.A. & Fike, D.A. (2019) Sea level, carbonate mineralogy, and early diagenesis controlled $\delta^{13}C$ records in Upper Ordovician carbonates. *Geology*, *48*, 194–199. https://doi.org/10.1130/G46861.1

Jost, A.B., Bachan, A., Van de Schootbrugge, B., Brown, S.T., DePaolo, D.J. & Payne, J.L. (2017) Additive effects of acidification and mineralogy on calcium isotopes in Triassic/Jurassic boundary limestones. *Geochemistry, Geophysics, Geosystems*, *18*, 113–124. https://doi.org/10.1002/2016GC006724.

Kiessling, W. (2015) Fuzzy seas. *Geology*, *43*, 191–192. https://doi.org/10.1130/focus022015.1.

Kimmig, S.R. & Holmden, C. (2017) Multi-proxy geochemical evidence for primary aragonite precipitation in a tropical-shelf 'calcite sea' during the Hirnantian glaciation. *Geochimica et Cosmochimica Acta*, *206*, 254–272. https://doi.org/10.1016/j.gca.2017.03.010

Knauth, L.P. & Kennedy, M.J. (2009) The late Precambrian greening of the Earth. *Nature*, *460*, 728–732. https://doi.org/10.1038/nature08213

Land, L.S. (1986) Limestone diagenesis—some geochemical considerations. *US Geological Survey Bulletin*, *1578*, 129–137.

Land, L.S., Behrens, E.W. & Frishman, S.A. (1979) The ooids of Baffin Bay, Texas. *Journal of Sedimentary Research*, *49*, 1269–1277.

Laya, J.C., Albader, A., Kaczmarek, S., Pope, M., Harris, P.M. & Miller, B. (2021) Dissolution of ooids in seawater-derived fluids – an example from Lower Permian re-sedimented carbonates, West Texas, USA. *Sedimentology*, *68*(6), 2671–2706. https://doi.org/10.1111/sed.12869

Lee, J. & Morse, J.W. (2010) Influences of alkalinity and pCO2 on $CaCO_3$ nucleation from estimated Cretaceous composition seawater representative of "calcite seas". *Geology*, *38*, 115–118. https://doi.org/10.1130/G30537.1

Logan, W.E. (1863) *Geology of Canada: geological survey of Canada, report progress from its commencement to 1863*. Montreal: Dawson Brothers, 983 pp.

Lowenstein, T.K., Timofeeff, M.N., Brennan, S.T., Hardie, L.A. & Demicco, R.V. (2001) Oscillations in Phanerozoic seawater chemistry: evidence from fluid inclusions. *Science*, *294*, 1086–1088. https://doi.org/10.1126/science.1064280

Machel, H.G. & Buschkuehle, B.E. (2008) Diagenesis of the Devonian Southesk-Cairn Carbonate Complex, Alberta, Canada: marine cementation, burial dolomitization, thermochemical sulfate reduction, anhydritization, and squeegee fluid flow. *Journal of Sedimentary Research*, *78*, 366–389. doi: https://doi.org/10.2110/jsr.2008.037

Mackenzie, F.T., Ver, L.M. & Lerman, A. (2000) Coastal-zone biogeochemical dynamics under global warming. *International Geology Review*, *42*, 193–206. https://doi.org/10.1080/0020681000946507

Martin, W.D., Fischer, H.J., Keogh, R.J. & Moorse, K. (1980) The petrology of the limestones in the Upper Gros Ventre and Gallatin Limestone Formations (Middle and Upper Cambrian) Northwestern Wind River Basin, Wyoming. Stratigraphy of Wyoming 31st Annual Field Conference Guidebook, pp. 37–51.

Neilson, J.E., Brasier, A.T. & North, C.P. (2016) Primary aragonite and high-Mg calcite in the late Cambrian (Furongian): potential evidence from marine carbonates in Oman. *Terra Nova*, *28*, 306–315. https://doi.org/10.1111/ter.12222

Odin, G.S. (1988) Green marine clays. *Developments in Sedimentology*, *45*, 444.

Palmer, A.R. & James, N.P. (1979) The Hawke Bay event: A circum-Iapetus regression near the lower Middle Cambrian boundary. Virginia Polytech Inst State Univ Dep Geol. Sci. Mem, 2, 15–18.

Pederson, C.L., Mavromatis, V., Dietzel, M., Rollion-Bard, C., Breitenbach, S.F.M., Yua, D., Nehrke, G. & Immenhauser,

A. (2020) Variation in the diagenetic response of aragonite archives to hydrothermal alteration. *Sedimentary Geology*, *406*, 105716–105732. https://doi.org/10.1016/j.sedgeo.2020.105716.

Pederson, C., Mavromatis, V., Dietzel, M., Rollion-Bard, C., Nehrke, G., Jons, N., Jochum, K.P. & Immenhauser, A. (2019) Diagenesis of mollusc aragonite and the role of fluid reservoirs. *Earth and Planetary Science Letters*, *514*, 130–142. https://doi.org/10.1016/j.epsl.2019.02.038.

Peters, S.E. & Gaines, R.R. (2012) Formation of the 'Great Unconformity' as a trigger for the Cambrian explosion. *Nature*, *484*, 363–366. https://doi.org/10.1038/nature10969

Pratt, B.R. & James, N.P. (1982) Cryptalgal-metazoan bioherms of early Ordovician age in the St. George Group, western Newfoundland. *Sedimentology*, *29*, 543–569.

Pulsipher, M.A., Schiffbauer, J.D., Jeffrey, M.J., Huntley, J.W., Fike, D.A. & Shelton, K.L. (2021) A meta-analysis of the Steptoean positive carbon isotope excursion: the SPICEraq database. *Earth Science Reviews*, *212*, 103442–103465. https://doi.org/10.1016/j.earscirev.2020.103442.

Rao, V.P. & Gopinathan, P. (2019) Late Quaternary sediments on the carbonate platform off western India: analogues of ancient platform carbonates. *Journal of Earth System Science*, *128*, 80–100. https://doi.org/10.1007/s12040-019-1112-y.

Richoz, S., van de Schootbrugge, B., Pross, J., Püttmann, W., Quan, T.M., Lindström, S., Heunisch, C., Fiebig, J., Maquil, R., Schouten, S., Hauzenberger, C.A. & Wignall, P. (2012) Hydrogen sulphide poisoning of shallow seas following the end-Triassic extinction. *Nature Geoscience*, *5*, 662–667. https://doi.org/10.1038/ngeo1539.

Riding, R. (2006) Cyanobacterial calcification Cyanobacterial calcification, carbon dioxide concentrating mechanisms, and Proterozoic-Cambrian changes in atmospheric composition. *Geobiology*, *4*, 299–316. https://doi.org/10.1111/j.1472-4669.2006.00087.x

Riding, R. (2011) Microbialites, stromatolites and thrombolites. In: Reitner, J. & Thiel, V. (Eds.) *Encylopedia of geobiology*. Dordrecht: Springer, pp. 635–654. https://doi.org/10.1007/978-1-4020-9212-1_19

Ries, J.B. (2009) Effects of secular variation in seawater mMg: Ca ratio (calcite-aragonite seas) on CaCo3 sediment production by the calcareous alga *Halimeda, Penicillu*s and *Udote*a – evidence from recent experiments and the geological record. *Terra Nova*, *21*, 323–339. https://doi.org/10.1111/j.1365-3121.2009.00899.x

Saltzman, M.R., Cowan, C.A., Runkel, A.C., Runnegar, B., Stewart, M.C. & Palmer, A.R. (2004) The Late Cambrian Spice (13C) Event and the Sauk II-SAUK III regression: new evidence from Laurentian Basins in Utah, Iowa, and Newfoundland. *Journal of Sedimentary Research*, *74*, 366–377. https://doi.org/10.1306/120203740366

Saltzman, M.R., Ripperdan, R.L., Brasier, M.D., Lohmann, K.C., Robison, R.A., Chang, W.T., Peng, S., Ergaliev, E.K. & Runnegar, B. (2000) A global carbon isotope excursion (SPICE) during the Late Cambrian: relation to trilobite extinctions, organic-matter burial and sea level. *Palaeogeography, Palaeoclimatology, Palaeoecology*, *162*, 211–223. https://doi.org/10.1016/S0031-0182(00)00128-0.

Saltzman, M.R., Runnegar, B. & Lohmann, K.C. (1998) Carbon isotope stratigraphy of upper Cambrian (Steptoean stage) sequences of the eastern Great Basin: record of a global oceanographic event. *Bulletin of the Geological Society of America*, *110*, 285–297. https://doi.org/10.1130/0016-7606(1998)110<0285:CISOUC>2.3.CO;2

Sandberg, P.A. (1983) An oscillating trend in Phanerozoic nonskeletal carbonate mineralogy. *Nature*, *305*, 19–22.

Schmid, S., Smith, P.M. & Woltering, M. (2018) A basin-wide record of the Late Cambrian Steptoean positive carbon isotope excursion (SPICE) in the Amadeus Basin, Australia. *Palaeogeography, Palaeoclimatology, Palaeoecology*, *508*, 116–128. https://doi.org/10.1016/j.palaeo.2018.07.027

Schuchert, C. & Dunbar, C.O. (1934) Stratigraphy of Western Newfoundland. *Geological Survey of America Memoir*, *1*, 123.

Stanley, S.M., Ries, J.B. & Hardie, L.A. (2010) Increased production of calcite and slower growth for the major sediment-producing alga Halimeda as the Mg/Ca ratio of seawater is lowered to a "calcite sea" level. *Journal of Sedimentary Research*, *80*, 6–16. https://doi.org/10.2110/jsr.2010.011

Tucker, M.E. & Wright, P. (1990) *Carbonate sedimentology*. Oxford: John Wiley & Sons, 496 pp. ISBN: 978-0-632-01472-9

Vulpius, S. & Kiessling, W. (2018) New constraints on the last aragonite–calcite sea transition from early Jurassic ooids. *Facies*, *64*, 1–9. https://doi.org/10.1007/s10347-017-0516-x.

Williams, H. (1979) Appalachian Orogen in Canada. *Canadian Journal of Earth Sciences*, *16*, 792–807. https://doi.org/10.1139/e79-070.

Zhuravlev, A.Y. & Wood, R.A. (2018) The two phases of the Cambrian explosion. *Science Reports*, *8*, 1–10. https://doi.org/10.1038/s41598-018-34962-y.

SUPPORTING INFORMATION

Additional supporting information may be found in the online version of the article at the publisher's website.

How to cite this article: Neilson JE, Barili R, Brasier A, De Ros LF, Ledingham S. The Steptoean Positive Carbon Isotope Excursion (SPICE), inorganic aragonite precipitation and sea water chemistry: Insights from the Middle–Late Cambrian Port au Port Group, Newfoundland. *Depositional Rec*. 2021;00:1–22. https://doi.org/10.1002/dep2.172